



UNIVERSITAT POLITÈCNICA DE CATALUNYA
BARCELONATECH

Escola Superior d'Enginyeries Industrial,
Aeroespacial i Audiovisual de Terrassa

ESEIAAT - UPC

Study for the computational resolution of conservation equations of mass, momentum and energy. Possible application to different aeronautical and industrial engineering problems: Case 1B

Report

Author: Laura Pla Olea

Director: Carlos David Perez Segarra

Co-Director: Asensio Oliva Llena

Degree: Grau en Enginyeria en Tecnologies Aeroespacials

Delivery date: 10-06-2017(Spring 2016-2017)

Contents

List of Tables	iv
List of Figures	v
1 Introduction	1
1.1 Aim	1
1.2 Scope	1
1.3 Requirements	2
1.4 Justification	2
1.4.1 Identification of the need	2
1.4.2 Advantatges and drawbacks	3
2 State of the art	4
2.1 Conservation equations	4
2.2 Numerical methods	5
2.3 Finite difference method	5
2.4 Finite volume method	6
2.4.1 Mesh	6
2.5 Time integration	7
2.6 Interpolation schemes	7
2.6.1 The central differencing scheme (CDS)	7
2.6.2 The upwind scheme (UDS)	8
2.6.3 The exponential scheme (EDS)	8
2.6.4 The hybrid scheme (HDS) and the power-law scheme (PLDS)	8
3 Conduction	9
3.1 Governing equations	9
3.2 Discretization	9
3.2.1 Spatial discretization	10
3.2.2 Temporal discretization	11
3.3 Boundary conditions	12
4 Four materials problem	13
4.1 Discretization	14

CONTENTS

4.2 Boundary conditions	14
4.3 Algorithm	16
4.4 Results	17
5 Convection	20
5.1 The generic convection-diffusion equation	20
5.2 Discretization	20
5.3 Evaluation of the value in the faces	22
6 Smith-Hutton problem	25
6.1 Discretization	26
6.2 Boundary conditions	26
6.3 Algorithm	26
6.4 Results	28
7 Fractional Step Method	32
7.1 The Helmholtz-Hodge decomposition theorem	32
7.2 Fractional Step Method algorithm	33
7.3 Discretization	33
7.3.1 Intermediate velocity discretization	33
7.3.2 Pressure discretization	36
7.3.3 Velocity discretization	36
7.4 Time step	37
8 Driven cavity problem	38
8.1 Discretization	38
8.2 Boundary conditions	39
8.3 Algorithm	40
8.4 Results	41
9 Differentially heated cavity	47
9.1 Natural convection	47
9.1.1 Non-dimensional equations	48
9.2 Application of the fractional step method	49
9.3 Discretization	49
9.4 Boundary conditions	50
9.5 Nusselt number	51
9.6 Algorithm	51
9.7 Results	53
10 Burgers' equation	58
10.1 Burgulence	59
10.2 Fourier space	59

CONTENTS

10.3 Discretization	61
10.3.1 Direct Numerical Simulation	62
10.3.2 Large-Eddy Simulation	62
10.4 Algorithm	63
10.5 Results	64
11 Square cylinder	65
11.1 Discretization	65
11.2 Boundary conditions	66
11.2.1 Inlet conditions	66
11.2.2 Outlet conditions	66
11.2.3 Wall conditions	66
11.3 Algorithm	67
11.4 Results	67
12 Conclusions	72
12.1 Future work	73
13 Economical, environmental and temporal considerations	74
13.1 Budget	74
13.2 Environmental impact	75
13.3 Planning	75
14 Bibliography	76

List of Tables

2.1	Particular cases of the convection-diffusion equation	5
4.1	Problem coordinates	13
4.2	Physical properties of the materials	14
4.3	Boundary conditions	14
4.4	Numerical parameters of the four materials problem	14
5.1	Function $A(P)$ for different schemes	24
6.1	Numerical parameters of the Smith-Hutton problem	26
6.2	Discretization coefficients of the boundary points	26
8.1	Numerical parameters of the driven cavity problem	38
8.2	Discretization coefficients in the boundary	39
9.1	Discretization coefficients of the boundary temperature nodes	51
9.2	Numerical parameters of the differentially heated cavity problem	53
9.3	Comparison between the benchmark solution and the calculated one	57
11.1	Numerical parameters of the square cylinder problem	66
13.1	Total cost of the study	74

List of Figures

2.1	Three successive grid points	6
2.2	Control volume (2D)	6
3.1	Heat fluxes through the faces of a control volume	10
4.1	General scheme of the four materials problem	13
4.2	Reference value: Instantaneous isotherms at $t=10000/2$ s	17
4.3	Instantaneous isotherms at $t=5000$ s	17
4.4	Instantaneous plot at $t=10000$ s	18
4.5	Instantaneous plot at $t=10000$ s for the homogeneous material M_2	19
4.6	Instantaneous plot at $t=10000$ s for the homogeneous material M_3	19
5.1	Mesh of the Smith-Hutton problem	21
6.1	General scheme of the Smith-Hutton problem	25
6.2	Distribution of ϕ at the output for $\rho/\Gamma = 10$	28
6.3	Distribution of ϕ at the output for $\rho/\Gamma = 10^3$	29
6.4	Distribution of ϕ at the output for $\rho/\Gamma = 10^6$	29
6.5	Representation of the whole domain for $\rho/\Gamma = 10$ (UDS)	30
6.6	Representation of the whole domain for $\rho/\Gamma = 10^3$ (UDS)	30
6.7	Representation of the whole domain for $\rho/\Gamma = 10^6$ (UDS)	31
7.1	Staggered meshes (2D)	34
7.2	Control volume of the horizontal velocity	35
7.3	Control volume of the vertical velocity	35
8.1	General scheme of the driven cavity problem	38
8.2	Comparison between the reference solution and the calculated one of the horizontal velocity along the vertical line in the geometric center of the cavity	42
8.3	Comparison between the reference solution and the calculated one of the vertical velocity along the horizontal line in the geometric center of the cavity	43
8.4	Horizontal velocity in the cavity	44
8.5	Vertical velocity in the cavity	45
8.6	Streamlines of the flow inside the cavity	46

9.1	General scheme of the differentially heated problem	47
9.2	Contour plots of the temperature	53
9.3	Contour plots of the horizontal velocity	54
9.4	Contour plots of the vertical velocity	55
9.5	Streamlines of the flow in the heated cavity	56
10.1	Schematic diagram of the energy cascade as a function of the size of the eddies	59
10.2	Representation of all the possible interactions between the modes in the convective term	61
10.3	Energy spectrum of the steady-state solution of the Burgers' equation	64
11.1	General scheme of the square cylinder problem	65
11.2	Horizontal velocity near the cylinder	68
11.3	Vertical velocity near the cylinder	69
11.4	Vertical velocity near the cylinder	70
11.5	Recirculation length vs. Reynolds number	71

1 | Introduction

1.1 Aim

The main objective of this paper is to provide knowledge in the computational resolution of the fundamental equations of fluid dynamics and mass and heat transfer by developing simulation codes. A second objective would be to apply the developed and verified codes to a specific case.

1.2 Scope

First, some basic cases concerning the equations of mass, momentum and energy are going to be solved in order to learn the fundamentals of the mathematical formulation and the computational and programming techniques that are going to be needed to develop the whole study. With the help of these cases, some simulation codes are going to be developed.

A second part of this paper is going to be the application of the knowledge acquired to a practical case.

In order to accomplish the objectives mentioned above, these are the following tasks to be developed:

- Previous research of the state of the art.
- Theoretical approach of the fluid dynamics behind all the cases and study of the mathematical formulation that should be applied.
- Development of the necessary numerical simulation tools. All the codes will need to be validated to ensure they are correct.
- Application of the acquired knowledge in simulation codes to an specific system.

- Analysis of the results.
- Conclusions.

1.3 Requirements

- Codes must be developed in C or C++.
- No external libraries or solvers can be used.
- Codes must be in a single file and compile with no errors.
- Codes must run without any input.
- Codes should be able to be executed in a normal computer.
- Simulations should provide realistic results.

1.4 Justification

1.4.1 Identification of the need

Conservation equations of mass, momentum and energy define the motion of fluids. Most thermal and engineering problems require to solve these equations to achieve the desired result. However, they are coupled differential equations, which means they are difficult to solve. Except for a few simplified cases, they usually do not have an analytical solution, so a numerical approach is often necessary. A huge amount of cases have been solved in the recent years, but there are still other problems that need to be studied and developed.

Since these equations need a numerical resolution in the majority of cases, the knowledge of computational techniques is essential to improve the simulations in accuracy and efficiency. A better understanding on the computational resolution of the conservation equations can lead to better results in the numerical simulations and with less computational cost. As a consequence, the actual knowledge in a variety of subjects could be improved, such as the temperature variation inside an engine or the way the air moves in the respiratory system. Furthermore, it could also lead to an optimization of different engineering systems; for example, more efficient wings for future airplanes.

1.4.2 Advantages and drawbacks

The main advantage of the approach explained in the scope is that the study of computational resolution starts from basic cases and its difficulty is upgraded with every case of fluid dynamics that is proposed. That way, the comprehension on the developed simulations is higher, which makes the codes more reliable. However, the simulation codes are being developed from zero. This is an advantage because no previous errors are going to be introduced on the program, but it is also a drawback because its development could take some time.

Anyhow, this project can be useful in the study of new engineering and thermal problems that need to be solved using the conservation equations of mass, momentum and energy; and can lead to other new studies of computational resolution of these equations.

2 | State of the art

The laws governing the processes of heat transfer and fluid flow are usually expressed in terms of differential equations. These equations are the momentum equation, the energy equation and the mass conservation equation, among others. However, these expressions don't have an analytical solution except for some simple cases. To solve complex problems it is necessary to use numerical methods.

2.1 Conservation equations

The three most important conservation equations are the mass conservation equation, the momentum conservation equation and the energy conservation equation:

$$\frac{\partial \rho}{\partial t} + \nabla \cdot (\rho \vec{v}) = 0 \quad (2.1)$$

$$\frac{\partial}{\partial t} (\rho \vec{v}) + \nabla \cdot (\rho \vec{v} \vec{v}) = -\nabla p + \nabla \cdot \vec{\tau} + \rho \vec{g} + \vec{f}^e \quad (2.2)$$

$$\frac{\partial}{\partial t} (\rho u) + \nabla \cdot (\rho \vec{v} u) = -\nabla \cdot \vec{q} - p \nabla \cdot \vec{v} + \vec{\tau} : \nabla \vec{v} + \Phi^e \quad (2.3)$$

These equations can be simplified depending on the case that is being studied. For example, for incompressible flows with no viscous dissipation, the energy conservation equation can be written as:

$$\rho c_p \left(\frac{\partial T}{\partial t} + \vec{v} \cdot \nabla T \right) = \nabla \cdot (\lambda \nabla T) \quad (2.4)$$

All these equations can be seen as a particular case of the generic convection-diffusion equation:

$$\frac{\partial}{\partial t} (\rho \phi) + \nabla \cdot (\rho \vec{v} \phi) = \nabla \cdot (\Gamma \nabla \phi) + S_{phi} \quad (2.5)$$

where ρ is the density, \vec{v} the velocity, Γ the diffusion coefficient, S_ϕ the source term, and ϕ the general variable that is going to be studied. Table 2.1 lists the values that these variables have to take in order to obtain the conservation equations previously mentioned.

Equation	ϕ	Γ	S_ϕ
Mass conservation	1	0	0
Momentum	\vec{v}	μ	$-\nabla p + \nabla \cdot \vec{r} + \rho \vec{g} + \vec{f}^e$
Energy (for a semiperfect gas)	u	λ/c_v	$-\nabla \cdot \vec{q} - p \nabla \cdot \vec{v} + \vec{r} : \nabla \vec{v} + \Phi^e$

Table 2.1: Particular cases of the convection-diffusion equation

2.2 Numerical methods

Numerical methods are based in dividing the domain that is going to be studied in different pieces. Instead of calculating the unknowns in the whole domain, they are studied in the finite number of points defined by these pieces: the grid points. This process is called discretization.

Once the domain is discretized, it is also necessary to discretize the equations. The relations between the grid points have to be established. It is assumed that the value ϕ of a grid point only influences the distribution of ϕ in its immediate neighbours. Consequently, as the number of grid points becomes larger, the numerical solution approaches the real solution of the problem.

2.3 Finite difference method

The finite difference method (FDM) is a discretization method based in the Taylor-series expansion. It is used to approximate the derivatives in the differential equation. Taking the three successive points represented in figure 2.1, the approximation of the values in the left point (west) and in the right point (east) is easily calculated with Taylor series:

$$\phi_W = \phi_P - \Delta x \left(\frac{d\phi}{dx} \right)_P + \frac{1}{2} (\Delta x)^2 \left(\frac{d^2\phi}{dx^2} \right) - \dots \quad (2.6)$$

$$\phi_E = \phi_P + \Delta x \left(\frac{d\phi}{dx} \right)_P + \frac{1}{2} (\Delta x)^2 \left(\frac{d^2\phi}{dx^2} \right) + \dots \quad (2.7)$$

Using a second order approximation and combining both expressions:

$$\left(\frac{d\phi}{dx} \right)_P \approx \frac{\phi_E - \phi_W}{2\Delta x} \quad (2.8)$$

$$\left(\frac{d^2\phi}{dx^2} \right)_P \approx \frac{\phi_W + \phi_E - 2\phi_P}{(\Delta x)^2} \quad (2.9)$$

These expressions are substituted in the differential equation to obtain the finite-differential equation. This approach is very simple, but it is not used in complex geometries. It also does not enforce conservation, as it is simply a mathematical approach.

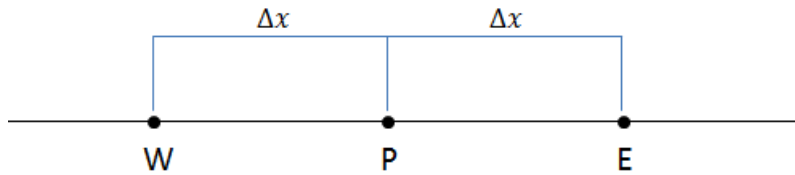


Figure 2.1: Three successive grid points

2.4 Finite volume method

The finite-volume method (FVM) is another discretization method more used than the FDM. It consists in dividing the domain in different control volumes as the ones in figure 2.2, so that each control volume surrounds one grid point. The differential equation is integrated over each control volume, ensuring that each of them satisfies the conservation principle. It is the method used in the present study.

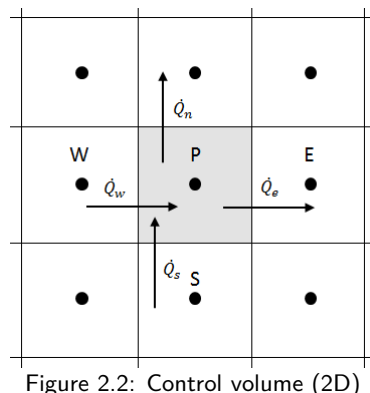


Figure 2.2: Control volume (2D)

2.4.1 Mesh

There are different ways to discretize the domain for the FVM. Some of these methods are listed below [1]:

- Structured (regular) mesh: Grid lines do not cross each other. Lines can be numbered consecutively, so that the position of any grid point can be easily identified by two (2D) or three (3D) indices. It is equivalent to a Cartesian grid. This is the simplest structure and easiest to work with, but it can only be used for geometrically simple domains.
- Unstructured mesh: The control volumes may have any shape, and there is not a restriction on the number of neighbour nodes. It is the method used for very complex geometries, but the grid generation and the pre-processing are more difficult than on structured meshes.

2.5 Time integration

Time is a one-way variable, which means that the unknowns only depend on the values in the previous instant of time, and do not depend on the values in the next instant of time. Knowing this property, to obtain the results of an unsteady problem, it is only necessary to discretize the time domain in time steps and calculate the values in each of them. When the unknowns of one time step are obtained, the calculation moves on to the next time step.

Time integration can be done using different methods. The ones that are widely used are:

- Explicit method: The simplest method. The terms are evaluated using the known values of the previous time step t^n . It is a first order approximation and easy to compute, but it requires very small time steps in order to achieve convergence.
- Implicit method: It is a very stable first order approximation, which makes it useful in problems with large time steps. The terms are evaluated with the values in the next instant of time t^{n+1} .
- Crank-Nicholson: It is a second order approximation. The terms are evaluated using the values of the previous and the next time step.

2.6 Interpolation schemes

In some cases, it is necessary to obtain the properties of the points that are not nodes. Some terms are evaluated in the faces, not in the nodes, so it is necessary to calculate the values of the variables in the faces of the control volume. There are different schemes to do so. Some of the most common ones are listed below [1, 2].

2.6.1 The central differencing scheme (CDS)

It is the most natural scheme. It is a linear interpolation between the two nearest nodes:

$$\phi_e - \phi_P = \frac{d_{Pe}}{d_{PE}} (\phi_E - \phi_P) \quad (2.10)$$

However, CDS is only valid in cases with low Reynolds number. It is a second order approximation, but may produce oscillatory solutions.

2.6.2 The upwind scheme (UDS)

It assumes that the value of ϕ in the interface is equal to the value of ϕ at the node on the upwind side of the face:

$$\begin{aligned}\phi_e &= \phi_P, & \text{if } \dot{m}_e > 0 \\ \phi_e &= \phi_E, & \text{if } \dot{m}_e < 0\end{aligned}\tag{2.11}$$

The solutions of the UDS are always physically realistic, but they may not be completely accurate because it is a first order approximation. However, this method is widely used due to its stability.

2.6.3 The exponential scheme (EDS)

Taking the generic convection-diffusion equation and assuming a steady one-dimensional problem with constant Γ and no source term, the analytic solution of the equation is an exponential function:

$$\frac{\phi - \phi_0}{\phi_L - \phi_0} = \frac{\exp(Px/L) - 1}{\exp(P) - 1}\tag{2.12}$$

where ϕ_0 and ϕ_L are the values of the function at $x = 0$ and $x = L$ respectively, and P is the Péclet number, a non-dimensional number:

$$P \equiv \frac{\rho u L}{\Gamma}\tag{2.13}$$

In the EDS, this analytic solution is used to determine the value on the faces, using the following expression:

$$\phi_e - \phi_P = \frac{\exp(P_e d_{Pe}/d_{PE}) - 1}{\exp(P_e) - 1} (\phi_E - \phi_P)\tag{2.14}$$

Though this solution is exact for the steady one-dimensional problem it is not for two or three-dimensional cases, unsteady problems and cases with source term, so it is not widely used.

2.6.4 The hybrid scheme (HDS) and the power-law scheme (PLDS)

Both methods are an approximation of the exponential function used in the EDS. Since exponentials are expensive to compute, the HDS and the PLDS are meant to provide a good result but with simpler functions. They divide the function given by the EDS in different parts and approximate the solution with simpler functions [2].

3 | Conduction

Conduction refers to the heat transfer through a solid or a stationary fluid [3]. It occurs due to the difference of temperatures between different parts of the solid, which generates a heat flux from the area with higher temperature to the one with lower temperature. It depends on the temperature gradient and on the physical properties of the material.

3.1 Governing equations

Conduction heat transfer in a solid is described by the energy equation 2.4. Since the domain is a solid, the velocity is equal to zero:

$$\rho c_P \frac{\partial T}{\partial t} = \nabla \cdot (\lambda \nabla T) + \dot{q}_v \quad (3.1)$$

where ρ is the density of the material, T the temperature, λ its conductivity, c_P its specific heat and \dot{q}_v its inner heat (source term).

However, a simpler approach is obtained with Fourier's law, which describes the heat transfer \vec{q} between two points in the direction \vec{n} :

$$\vec{q} = -\lambda \frac{\partial T}{\partial n} \vec{n} \quad (3.2)$$

3.2 Discretization

To discretize the equation, the finite volume method is used, dividing the domain with a Cartesian grid. The domain is discretized using the node centred distribution, to avoid having conflictive control volumes between the different materials.

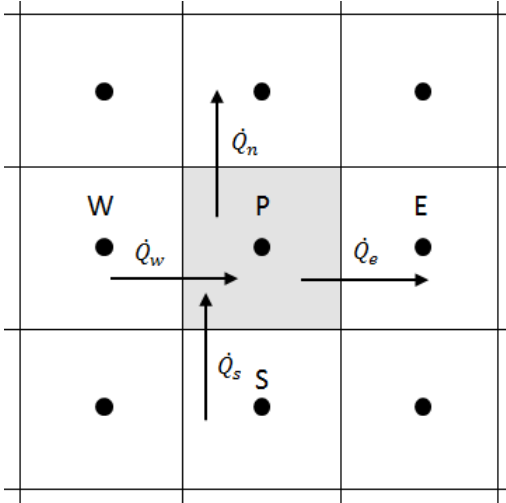


Figure 3.1: Heat fluxes through the faces of a control volume

3.2.1 Spatial discretization

The heat fluxes through the walls represented in figure 3.1 are given by equation 3.2. They are obtained integrating the expression in the vertical and horizontal directions.

$$\dot{Q}_e = - \int^{S_e} \lambda \frac{\partial T}{\partial x} dS \approx - \left(\lambda \frac{\partial T}{\partial x} \right)_e S_e \approx -\lambda_e \frac{T_E - T_P}{d_{PE}} S_e \quad (3.3)$$

$$\dot{Q}_w = - \int^{S_w} \lambda \frac{\partial T}{\partial x} dS \approx - \left(\lambda \frac{\partial T}{\partial x} \right)_w S_w \approx -\lambda_w \frac{T_P - T_W}{d_{PW}} S_w \quad (3.4)$$

$$\dot{Q}_n = - \int^{S_n} \lambda \frac{\partial T}{\partial y} dS \approx - \left(\lambda \frac{\partial T}{\partial y} \right)_n S_n \approx -\lambda_n \frac{T_N - T_P}{d_{PN}} S_n \quad (3.5)$$

$$\dot{Q}_s = - \int^{S_s} \lambda \frac{\partial T}{\partial y} dS \approx - \left(\lambda \frac{\partial T}{\partial y} \right)_s S_s \approx -\lambda_s \frac{T_P - T_S}{d_{PS}} S_s \quad (3.6)$$

where d is the distance between two nodes and S the surface of the given face of the control volume.

The inner heat of the material can be discretized as:

$$\dot{Q}_{VP} = \int_{V_P} \dot{q}_v dV \approx \dot{q}_{vP} V_P \quad (3.7)$$

In the heat fluxes, though, the conductivity can have two different values: one on the left node and another one on the right node. Taking the value of the conductivity of just one node could lead to non-realistic results, because the heat fluxes evaluate the gradient of temperatures from one node to the other. To avoid this problem, the conductivity is determined using the harmonic mean:

$$\lambda_e = \frac{d_{PE}}{\frac{1}{\lambda_P} + \frac{1}{\lambda_E}} \quad (3.8)$$

3.2.2 Temporal discretization

Time discretization is done using the First law of thermodynamics:

$$\int_{V_P} \rho \frac{\partial u}{\partial t} dV = \sum \dot{Q}_P \quad (3.9)$$

where u is the internal energy of the control volume. Assuming an incompressible material, the First law of thermodynamics is integrated over time. Taking n as the previous instant of time and $n + 1$ the instant of time that is going to be calculated:

$$\int_{t^n}^{t^{n+1}} \rho_P \frac{\partial \bar{u}_P}{\partial t} V_P dt = \int_{t^n}^{t^{n+1}} \sum \dot{Q}_P dt \quad (3.10)$$

Rearranging the first term of the equation:

$$\begin{aligned} \int_{t^n}^{t^{n+1}} \rho_P \frac{\partial \bar{u}_P}{\partial t} V_P dt &= \rho_P V_P (\bar{u}_P^{n+1} - \bar{u}_P^n) \approx \\ &\rho_P V_P (u_P^{n+1} - u_P^n) = \rho_P V_P \bar{c}_P (T_P^{n+1} - T_P^n) \end{aligned} \quad (3.11)$$

To integrate the second term of the equation over time, a new variable β is introduced, so as to be able to use an implicit ($\beta = 1$), explicit ($\beta = 0$) or Crank-Nicholson scheme ($\beta = 0.5$).

$$\int_{t^n}^{t^{n+1}} \sum \dot{Q}_P dt = [\beta \sum \dot{Q}_P^{n+1} + (1 - \beta) \sum \dot{Q}_P^n] \Delta t \quad (3.12)$$

The discretized equation is finally obtained as the sum of both terms:

$$\rho_P V_P \bar{c}_P \frac{T_P^{n+1} - T_P^n}{\Delta t} = \beta \sum \dot{Q}_P^{n+1} + (1 - \beta) \sum \dot{Q}_P^n \quad (3.13)$$

where

$$\begin{aligned} \dot{Q}_P &= -\dot{Q}_w + \dot{Q}_e - \dot{Q}_s + \dot{Q}_n + \dot{q}_{vP} V_P = \\ &- \lambda_w \frac{T_P - T_W}{d_{PW}} S_w + \lambda_e \frac{T_E - T_P}{d_{PE}} S_e - \lambda_s \frac{T_P - T_S}{d_{PS}} S_s + \lambda_n \frac{T_N - T_P}{d_{PN}} S_n + \dot{q}_{vP} V_P \end{aligned} \quad (3.14)$$

To simplify the equation, it can be rewritten with coefficients dependant on the properties of the nearest nodes in the following form:

$$a_P T_P = a_E T_E + a_W T_W + a_N T_N + a_S T_S + b_P \quad (3.15)$$

These discretization coefficients are different for each node, and have the following values:

$$a_E = \beta \frac{\lambda_e S_e}{d_{PE}} \quad (3.16)$$

$$a_W = \beta \frac{\lambda_w S_w}{d_{PW}} \quad (3.17)$$

$$a_N = \beta \frac{\lambda_n S_n}{d_{PN}} \quad (3.18)$$

$$a_S = \beta \frac{\lambda_s S_s}{d_{PS}} \quad (3.19)$$

$$a_P = a_E + a_W + a_N + a_S + \rho_P V_P \bar{c}_P / \Delta t \quad (3.20)$$

$$\begin{aligned} b_P = & \frac{\rho_P V_P \bar{c}_P T_P^n}{\Delta t} + \beta \dot{q}_{vP}^{n+1} V_P + \\ & (1 - \beta) \left[-\lambda_w \frac{T_P - T_W}{d_{PW}} S_w + \lambda_e \frac{T_E - T_P}{d_{PE}} S_e - \lambda_s \frac{T_P - T_S}{d_{PS}} S_s + \lambda_n \frac{T_N - T_P}{d_{PN}} S_n + \dot{q}_{vP} V_P \right]^n \end{aligned} \quad (3.21)$$

3.3 Boundary conditions

There are three kinds of boundary conditions that are common in conduction problems [3]:

- Constant surface temperature: The temperature of a surface is prescribed. The condition is fulfilled just by substituting the value of the prescribed temperature in the conduction equation.

$$T_{wall} = T_{prescribed} \quad (3.22)$$

- Constant surface heat flux: The heat flux in a surface is prescribed. In this case, the condition is imposed just by adding the heat flux to the conduction equation.

$$\dot{q}_{wall} = \dot{q}_{prescribed} \quad (3.23)$$

- Convection surface condition: This boundary condition refers to the existence of convection heat transfer at the surface. To fulfil this condition, it is necessary to calculate the heat transfer due to the convection:

$$\dot{q}_{conduction} = -\lambda \frac{T_{node} - T_{wall}}{d_{nw}} \quad (3.24)$$

$$\dot{q}_{convection} = \alpha (T_g - T_{wall}) \quad (3.25)$$

$$\dot{q}_{conduction} = \dot{q}_{convection} \quad (3.26)$$

$$\dot{q} = \frac{T_g - T_{node}}{\frac{1}{\alpha} + \frac{d_{nw}}{\lambda}} \quad (3.27)$$

where T_g is the temperature of the fluid next to the wall, α the convection heat transfer coefficient, T_{node} the temperature of the node next to the wall, and d_{nw} the distance from the node to the wall.

4 | Four materials problem

The four materials problem is a two-dimensional transient conduction problem. It consists in a long rod composed of four different materials with different properties. The general scheme of the problem is represented in figure 4.1, and the dimensions of the materials, their properties, and the boundary conditions are in the tables below.

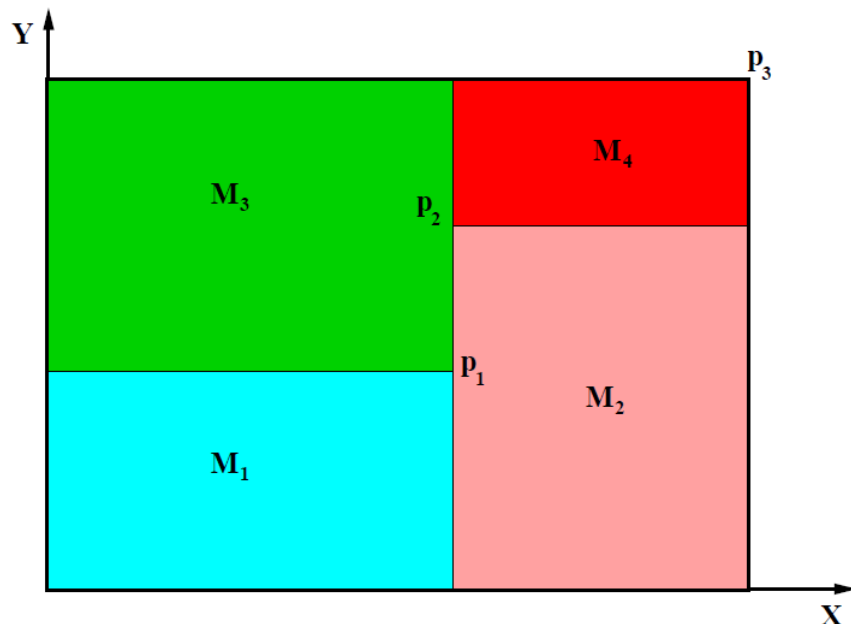


Figure 4.1: General scheme of the four materials problem

	x [m]	y [m]
p_1	0.50	0.40
p_2	0.50	0.70
p_3	1.10	0.80

Table 4.1: Problem coordinates

Since it is a transient problem, it is necessary to know the temperature at $t = 0$. The initial temperature field is $T = 8.00^\circ C$.

	$\rho [kg/m^3]$	$c_P [J/kgK]$	$\lambda [W/mK]$
M_1	1500.00	750.00	170.00
M_2	1600.00	770.00	140.00
M_3	1900.00	810.00	200.00
M_4	2500.00	930.00	140.00

Table 4.2: Physical properties of the materials

Cavity wall	Boundary condition
Bottom	Isotherm at $T = 23.00^\circ C$
Top	Uniform $Q_{flow} = 60.00 W/m$ length
Left	In contact with a fluid at $T_g = 33.00^\circ C$ and heat transfer coefficient $9.00 W/m^2 K$
Right	Uniform temperature $T = 8.00 + 0.005t^\circ C$ (where t is the time in seconds)

Table 4.3: Boundary conditions

4.1 Discretization

The spatial discretization of the problem is that described in section 3.2.1. However, since there are different materials, each of them is discretized separately. The variable M_1 is the number of control volumes in the vertical direction from $Y = 0$ to the point p_1 , M_2 from p_1 to p_2 and M_3 from p_2 to p_3 . In the horizontal direction, the variable N_1 is the number of control volumes from $X = 0$ to the point p_1 and N_2 from p_1 to p_3 . The precision used in the convergence criterion is given by δ .

M_1	M_2	M_3	N_1	N_2	β	δ
40	30	10	50	60	0.5	10^{-3}

Table 4.4: Numerical parameters of the four materials problem

4.2 Boundary conditions

The coefficients of the discretized equation in the inner nodes are the ones of the section 3.2.2. However, the outer walls of the rod have special conditions, so each of them has to be studied in order to determine which coefficients of their boundary nodes are different.

In the left wall, there is convection with the fluid outside of the road. To fulfil this condition, some coefficients have to be recalculated:

$$a_W = 0 \quad (4.1)$$

$$a_P = a_E + a_W + a_N + a_S + \frac{\rho_P V_P \bar{c}_P}{\Delta t} + \frac{\beta}{\frac{1}{\alpha} + \frac{d_{Pw}}{\lambda_P}} \quad (4.2)$$

$$b_P = \frac{\rho_P V_P \bar{c}_P T_P^n}{\Delta t} + \beta \left(\dot{q}_{vP}^{n+1} V_P + \frac{T_g}{\frac{1}{\alpha} + \frac{d_{Pw}}{\lambda_P}} \right) \\ + (1 - \beta) \left[\frac{T_g - T_P}{\frac{1}{\alpha} + \frac{d_{Pw}}{\lambda_P}} + \lambda_e \frac{T_E - T_P}{d_{PE}} S_e - \lambda_s \frac{T_P - T_S}{d_{PS}} S_s + \lambda_n \frac{T_N - T_P}{d_{PN}} S_n + \dot{q}_{vP} V_P \right]^n \quad (4.3)$$

There is a constant heat flux in the top wall. The value of this flux is given for the total wall, so it is assumed that it is uniformly distributed over the top wall. In this case, the coefficients that change their value are:

$$a_N = 0 \quad (4.4)$$

$$b_P = \frac{\rho_P V_P \bar{c}_P T_P^n}{\Delta t} + \beta \dot{q}_{vP}^{n+1} V_P + Q_{flow} \frac{S_n}{S_{top}} \\ + (1 - \beta) \left[-\lambda_w \frac{T_P - T_W}{d_{PW}} S_w + \lambda_e \frac{T_E - T_P}{d_{PE}} S_e - \lambda_s \frac{T_P - T_S}{d_{PS}} S_s + \dot{q}_{vP} V_P \right]^n \quad (4.5)$$

In the right wall, the temperature T_r is given, and it changes over time. The coefficients are very similar to those of the general case. The only differences are:

$$a_E = 0 \quad (4.6)$$

$$a_P = a_E + a_W + a_N + a_S + \frac{\rho_P V_P \bar{c}_P}{\Delta t} + \beta \frac{\lambda_P S_e}{d_{Pe}} \quad (4.7)$$

$$b_P = \frac{\rho_P V_P \bar{c}_P T_P^n}{\Delta t} + \beta \left(\dot{q}_{vP}^{n+1} V_P + \frac{\lambda_P S_e}{d_{Pe}} T_r^{n+1} \right) \\ + (1 - \beta) \left[-\lambda_w \frac{T_P - T_W}{d_{PW}} S_w + \lambda_P \frac{T_r - T_P}{d_{Pe}} S_e - \lambda_s \frac{T_P - T_S}{d_{PS}} S_s + \lambda_n \frac{T_N - T_P}{d_{PN}} S_n + \dot{q}_{vP} V_P \right]^n \quad (4.8)$$

Finally, in the bottom wall, the temperature T_b is also given, but it is constant over time. The approach is very similar to that of the right wall, so that the different coefficients are:

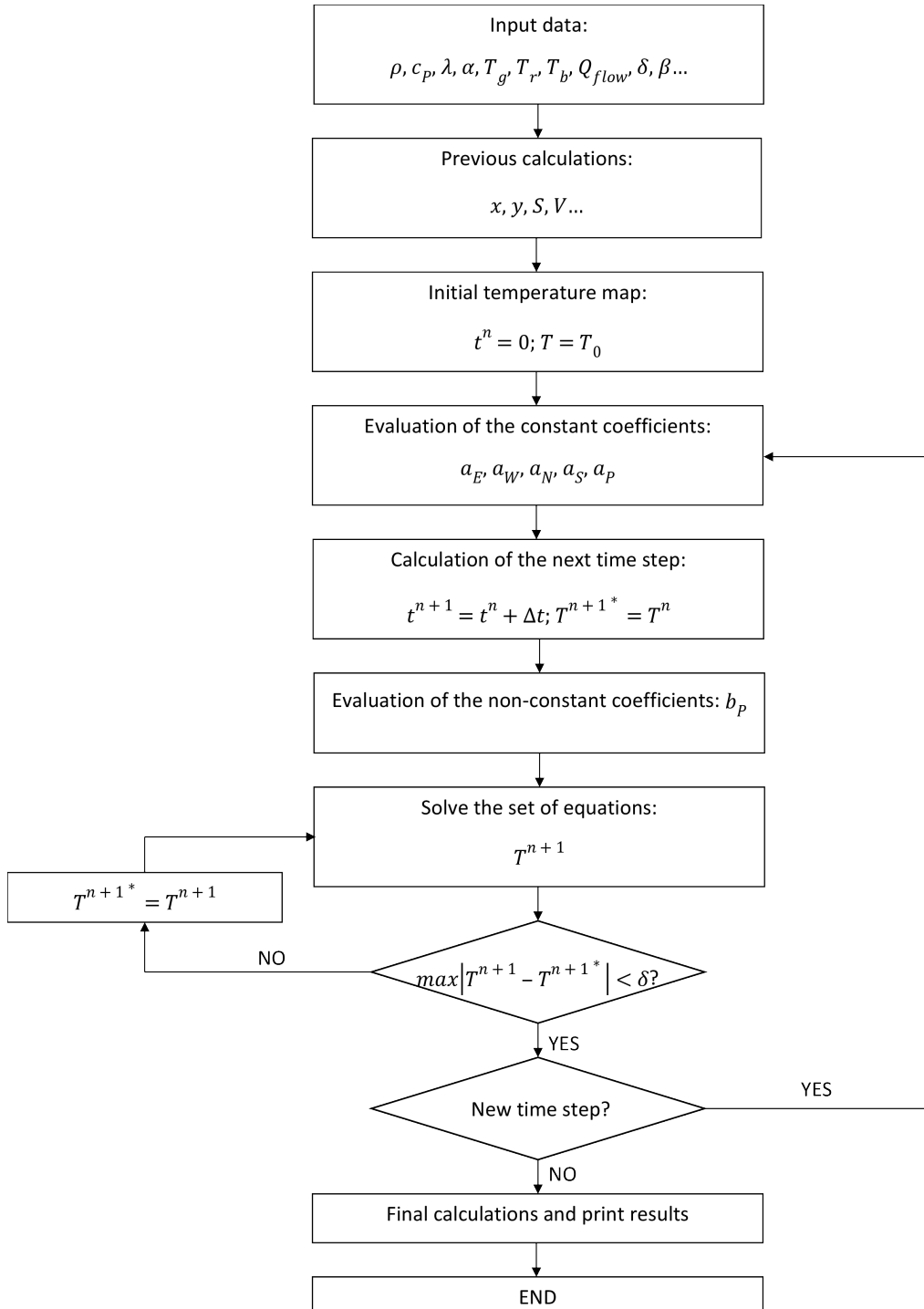
$$a_S = 0 \quad (4.9)$$

$$a_P = a_E + a_W + a_N + a_S + \frac{\rho_P V_P \bar{c}_P}{\Delta t} + \beta \frac{\lambda_P S_s}{d_{Ps}} \quad (4.10)$$

$$b_P = \frac{\rho_P V_P \bar{c}_P T_P^n}{\Delta t} + \beta \left(\dot{q}_{vP}^{n+1} V_P + \frac{\lambda_P S_s}{d_{Ps}} T_b \right) \\ + (1 - \beta) \left[-\lambda_w \frac{T_P - T_W}{d_{PW}} S_w + \lambda_e \frac{T_E - T_P}{d_{PE}} S_e - \lambda_P \frac{T_P - T_b}{d_{Ps}} S_s + \lambda_n \frac{T_N - T_P}{d_{PN}} S_n + \dot{q}_{vP} V_P \right]^n \quad (4.11)$$

4.3 Algorithm

The algorithm used in this convection problem is represented below. In this case, some of the discretization coefficients are constant, but they usually change over time. These would change slightly the algorithm used.



4.4 Results

To verify the simulation, the results obtained are compared with the reference values for a time of $t=5000$ s. As it can be seen in figures 4.2 and 4.2, the results of the code are very similar to the reference values. The biggest differences are the isotherms of 23 and 24°.

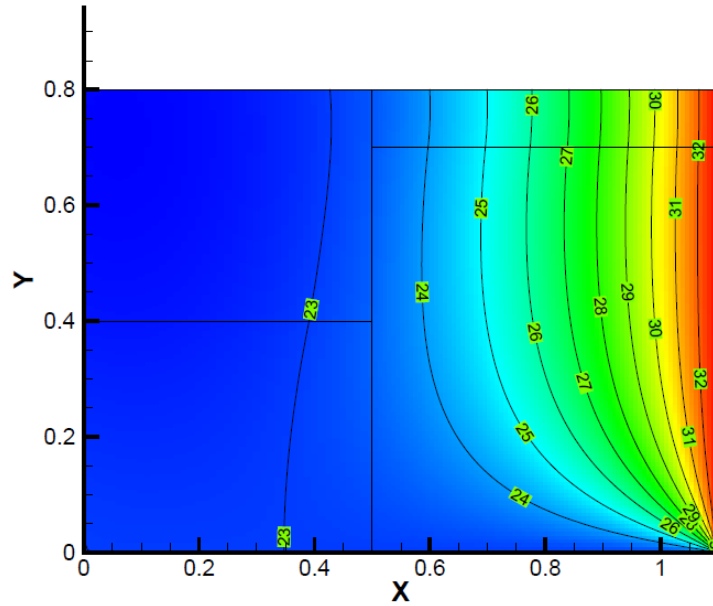


Figure 4.2: Reference value: Instantaneous isotherms at $t=10000/2$ s

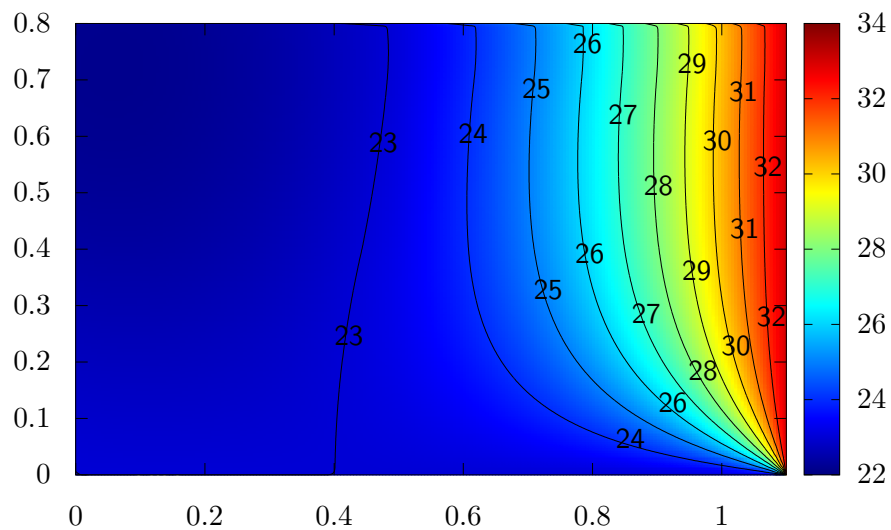


Figure 4.3: Instantaneous isotherms at $t=5000$ s

Since the temperature in the right wall changes over time, the four materials problem never reaches a steady state. However, to see the evolution of the temperature, the simulation has been run for a final time of $t = 10000\text{s}$, obtaining the results of the figure 4.4.

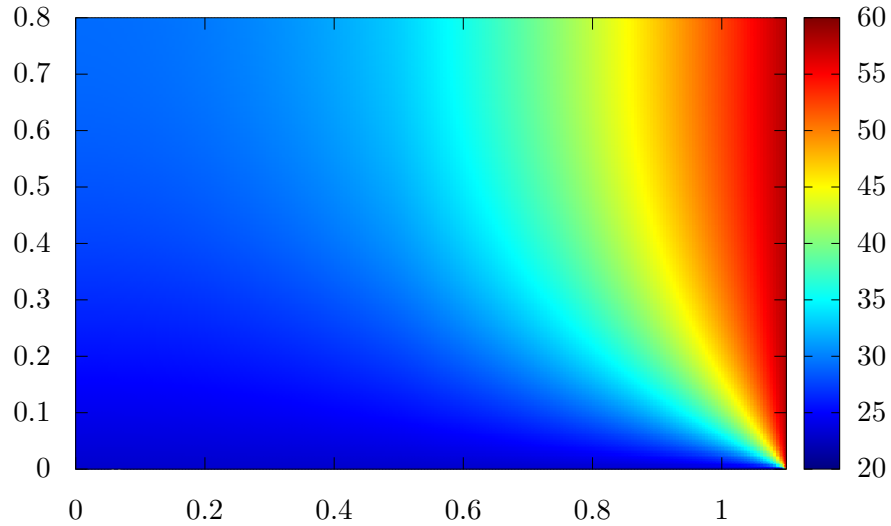


Figure 4.4: Instantaneous plot at $t=10000\text{s}$

Comparing the solutions at 5000 s and at 10000 s, it can be seen that the whole rod has increased its temperature, but the gradient of temperature between the left and right walls has doubled. Another important difference is that hot temperatures move to the left as time passes.

In addition, to further analyse the results obtained, the same simulation has been run for two rods of homogeneous material. The geometrical parameters and the boundary conditions have been maintained, but the physical properties of the whole material are those of the section M_2 (figure 4.5) and M_3 (figure 4.6) respectively of the four materials problem.

Comparing the graphs, it can be stated that the final result is very similar in all three cases. In the case of the M_2 material, the main visible difference is that in the four materials problem, higher temperatures move further to the left. In the original problem, the upper right region is made of the material M_4 , which has the same conductivity as the homogeneous material M_2 , but a higher density and specific heat.

In the case of the homogeneous M_3 material, it can be seen that it is the material that has better conductivity, because hotter temperatures move slightly further to the left in the upper zone compared to the results of the original problem.

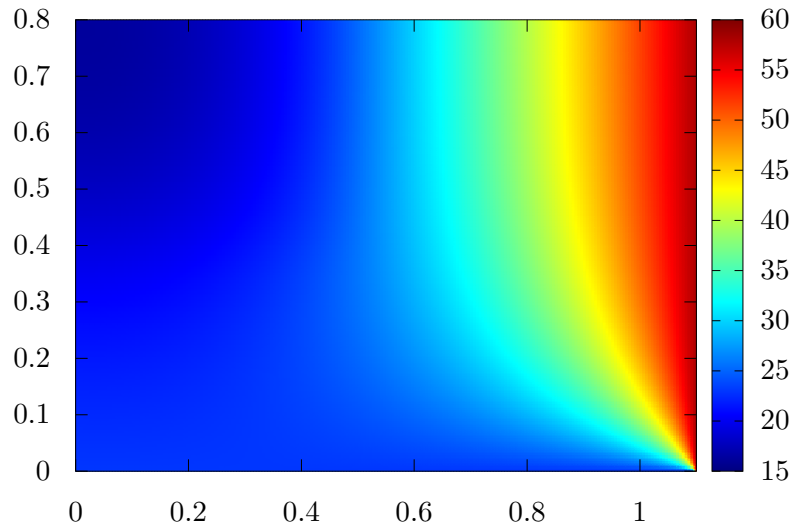


Figure 4.5: Instantaneous plot at $t=10000$ s for the homogeneous material M_2

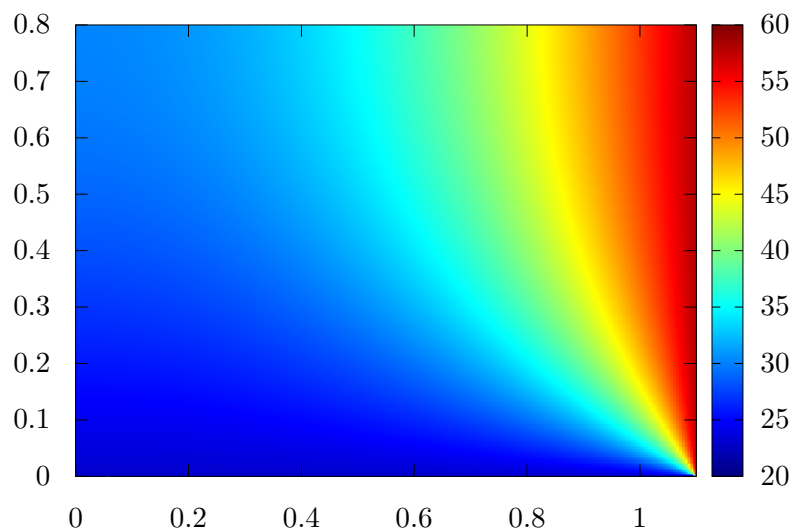


Figure 4.6: Instantaneous plot at $t=10000$ s for the homogeneous material M_3

5 | Convection

Convective heat transfer is the study of heat transport processes due to the flow of fluids [4]. Inside a fluid there may be different temperatures: some parts of it can have a higher temperature and others a lower temperature. The movement of liquids or gases combined with the temperature gradient causes convection [3].

This heat transfer occurs in the layers of a fluid, or can also occur between a solid and the fluid that is in contact with it. In both cases, the heat transfer depends on the properties of the fluid and its motion. As a consequence, to understand the heat transfer in a fluid or between a solid and a fluid, it is necessary to know the properties of the fluid itself.

5.1 The generic convection-diffusion equation

The motion of a fluid is described by the Navier-Stokes equations or conservation equations. As discussed in section 2.1, the Navier-Stokes equations are a particular case of the generic convection-diffusion equation 5.1:

$$\frac{\partial}{\partial t} (\rho\phi) + \nabla \cdot (\rho\vec{v}\phi) = \nabla \cdot (\Gamma\nabla\phi) + S_{phi} \quad (5.1)$$

where ρ is the density, \vec{v} the velocity, Γ the diffusion coefficient, S_ϕ the source term, and ϕ the general variable that is going to be studied.

5.2 Discretization

It is necessary to discretize equation 5.1 in space and time. The spatial discretization is done dividing the domain in different control volumes with a Cartesian grid. The node centred distribution is used, as specified in figure 5.1. The boundary nodes are in blue and the inner nodes in black.

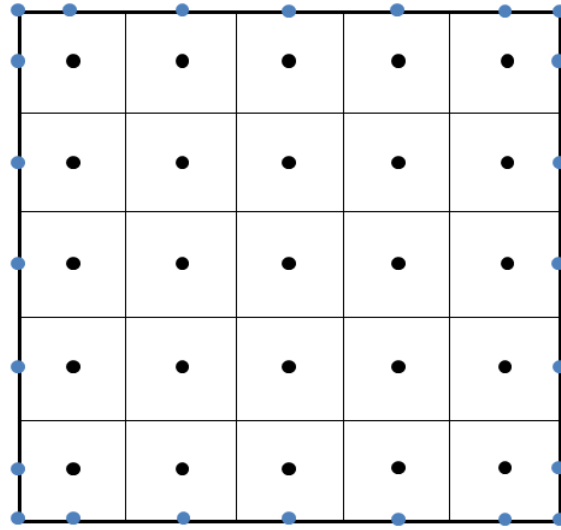


Figure 5.1: Mesh of the Smith-Hutton problem

To do so, it is easier to start with the discretization of the mass equation:

$$\frac{\partial \rho}{\partial t} + \nabla \cdot (\rho \vec{v}) = 0 \quad (5.2)$$

The first step is to integrate it over time and space. Taking only the first term of the equation:

$$\int_{t^n}^{t^{n+1}} \int_{V_P} \frac{\partial \rho}{\partial t} dV dt = \int_{t^n}^{t^{n+1}} V_P \frac{\partial \bar{\rho}_P}{\partial t} dt = V_P (\bar{\rho}_P^{n+1} - \bar{\rho}_P^n) \approx V_P (\rho_P^{n+1} - \rho_P^n) = V_P (\rho_P - \rho_0) \quad (5.3)$$

Using the Divergence Theorem, the second term of the mass equation transforms into a surface integral. Then, to integrate over time, an implicit scheme is used:

$$\begin{aligned} \int_{t^n}^{t^{n+1}} \int_{V_P} \nabla \cdot (\rho \vec{v}) dV dt &= \int_{t^n}^{t^{n+1}} \int_{S_f} \rho \vec{v} \cdot \vec{n} dS dt = \\ &\int_{t^n}^{t^{n+1}} (\dot{m}_e - \dot{m}_w + \dot{m}_n - \dot{m}_s) dt \approx [\dot{m}_e - \dot{m}_w + \dot{m}_n - \dot{m}_s]^{n+1} \Delta t \end{aligned} \quad (5.4)$$

The final discretized mass equation is 5.5:

$$\frac{V_P (\rho_P - \rho_0)}{\Delta t} + \dot{m}_e - \dot{m}_w + \dot{m}_n - \dot{m}_s = 0 \quad (5.5)$$

The discretization of the convection-diffusion equation is very similar to that of the mass equation. The time integration is also done using an implicit scheme, but the integration over space requires a further analysis.

Integrating over the volume the transport term of equation 5.1 and applying the Divergence Theorem:

$$\int_{V_P} \nabla \cdot (\rho \vec{v} \phi) = \int_{S_f} \rho \phi \vec{v} \cdot \vec{n} dS = \dot{m}_e \phi_e - \dot{m}_w \phi_w + \dot{m}_n \phi_n - \dot{m}_s \phi_s \quad (5.6)$$

The same procedure is done for the diffusion term:

$$\int_{V_P} \nabla \cdot (\Gamma \nabla \phi) = \int_{S_f} \Gamma \cdot \nabla \phi \cdot \vec{n} dS = -\Gamma_w \frac{\partial \phi}{\partial x} \Big|_w S_w + \Gamma_e \frac{\partial \phi}{\partial x} \Big|_e S_e - \Gamma_s \frac{\partial \phi}{\partial x} \Big|_s S_s + \Gamma_n \frac{\partial \phi}{\partial x} \Big|_n S_n \approx D_e (\phi_E - \phi_P) - D_w (\phi_P - \phi_W) + D_n (\phi_N - \phi_P) - D_s (\phi_P - \phi_S) \quad (5.7)$$

where the diffusion conductances are

$$D_e = \frac{\Gamma_e S_e}{d_{PE}} \quad (5.8)$$

$$D_w = \frac{\Gamma_w S_w}{d_{PW}} \quad (5.9)$$

$$D_n = \frac{\Gamma_n S_n}{d_{PN}} \quad (5.10)$$

$$D_s = \frac{\Gamma_s S_s}{d_{PS}} \quad (5.11)$$

Finally, to simplify the source term, it is linearized:

$$\int_{V_P} S_\phi dV \approx S_{\phi,P} V_P = (S_c^\phi + S_p^\phi \phi_P) V_P \quad (5.12)$$

So that the resulting discretized equation is:

$$\frac{\rho_P \phi_P - \rho_P^0 \phi_P^0}{\Delta t} V_P + \dot{m}_e \phi_e - \dot{m}_w \phi_w + \dot{m}_n \phi_n - \dot{m}_s \phi_s = D_e (\phi_E - \phi_P) - D_w (\phi_P - \phi_W) + D_n (\phi_N - \phi_P) - D_s (\phi_P - \phi_S) + S_{\phi,P} V_P \quad (5.13)$$

Multiplying by ϕ the discretized mass equation 5.5 and subtracting the result in 5.13, the final discretized convection-diffusion equation is obtained:

$$\rho_P^0 \frac{\phi_P - \phi_P^0}{\Delta t} V_P + \dot{m}_e (\phi_e - \phi_P) - \dot{m}_w (\phi_w - \phi_P) + \dot{m}_n (\phi_n - \phi_P) - \dot{m}_s (\phi_s - \phi_P) = D_e (\phi_E - \phi_P) - D_w (\phi_P - \phi_W) + D_n (\phi_N - \phi_P) - D_s (\phi_P - \phi_S) + S_{\phi,P} V_P \quad (5.14)$$

The final step is to find an expression to evaluate the required properties in the faces of the control volume.

5.3 Evaluation of the value in the faces

To simplify the problem, a new variable is introduced to the problem: the total flux [2]. This variable is split in the two dimensions of the problem, the flux in the x-direction and the flux in the y-direction:

$$J_x \equiv \rho u \phi - \Gamma \frac{\partial \phi}{\partial x} \quad (5.15)$$

$$J_y \equiv \rho v \phi - \Gamma \frac{\partial \phi}{\partial y} \quad (5.16)$$

Introducing the expressions of the total flux into equation 5.14, the discretized convection diffusion equation becomes:

$$\rho_P^0 \frac{\phi_P - \phi_P^0}{\Delta t} V_P + (J_e - F_e \phi_P) - (J_w - F_w \phi_P) + (J_n - F_n \phi_P) - (J_s - F_s \phi_P) = \\ (S_p^\phi \phi_P) V_P \quad (5.17)$$

where the flow rates are:

$$F_e = (\rho u)_e S_e \quad (5.18)$$

$$F_w = (\rho u)_w S_w \quad (5.19)$$

$$F_n = (\rho v)_n S_n \quad (5.20)$$

$$F_s = (\rho v)_s S_s \quad (5.21)$$

However, it is necessary to know how the fluxes are going to be evaluated. In order to use non-dimensional numbers, a new variable is defined:

$$J^* \equiv \frac{J \delta}{\Gamma} = P \phi - \frac{d \phi}{d(x/\delta)} \quad (5.22)$$

where P is the Péclet number and δ is the distance between the point that is going to be studied i , and the point next to it, $i+1$. The variable ϕ and the gradient $d\phi/d(x/\delta)$ are a combination of ϕ_i and ϕ_{i+1} , so that J^* can be expressed as [2]:

$$J^* = B \phi_i - A \phi_{i+1} \quad (5.23)$$

Coefficients A and B are dimensionless and depend on the Péclet number. Taking some of their properties into account and introducing the operator $\llbracket A, B \rrbracket$ that denotes the greater of A and B [2], it can be deduced that:

$$A(P) = A(|P|) + \llbracket -P, 0 \rrbracket \quad (5.24)$$

$$B(P) = A(|P|) + \llbracket P, 0 \rrbracket \quad (5.25)$$

Introducing equations 5.24 and 5.25 into 5.17, the following formulation is obtained:

$$a_P \phi_P = a_E \phi_E + a_W \phi_W + a_N \phi_N + a_S \phi_S + b_P \quad (5.26)$$

where

$$a_E = D_e A(|P_e|) + \llbracket -F_e, 0 \rrbracket \quad (5.27)$$

$$a_W = D_w A(|P_w|) + \llbracket F_w, 0 \rrbracket \quad (5.28)$$

$$a_N = D_n A(|P_n|) + \llbracket -F_n, 0 \rrbracket \quad (5.29)$$

$$a_S = D_s A(|P_s|) + \llbracket -F_s, 0 \rrbracket \quad (5.30)$$

$$a_P = a_E + a_W + a_N + a_S + \frac{\rho_P^0 V_P}{\Delta t} - S_P V_P \quad (5.31)$$

$$b_P = S_c V_P + \frac{\rho_P^0 V_P}{\Delta t} \phi_P^0 \quad (5.32)$$

And the Péclet numbers are:

$$P_e = \frac{F_e}{D_e} \quad (5.33)$$

$$P_w = \frac{F_w}{D_w} \quad (5.34)$$

$$P_n = \frac{F_n}{D_n} \quad (5.35)$$

$$P_s = \frac{F_s}{D_s} \quad (5.36)$$

The only operator that remains undefined is the coefficient A . Its value depends on the integration scheme that is going to be used. Some of its values are listed in table 5.1.

Scheme	Formula for $A(P_s)$
Central difference (CDS)	$1 - 0.5 P $
Upwind (UDS)	1
Hybrid (HDS)	$\llbracket 0, 1 - 0.5 P \rrbracket$
Power law (PLDS)	$\llbracket 0, (1 - 0.5 P)^5 \rrbracket$
Exponential (EDS)	$ P / [\exp(P) - 1]$

Table 5.1: Function $A(|P|)$ for different schemes. Extracted from [2]

6 | Smith-Hutton problem

The Smith-Hutton problem is a two-dimensional steady convection-diffusion problem, represented in figure 6.1. The density is constant, and the velocity field is known.

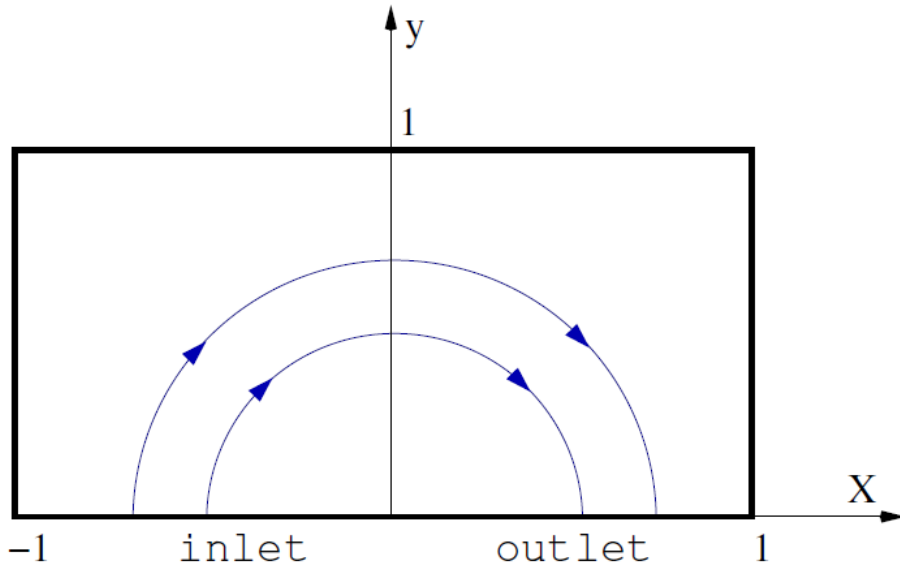


Figure 6.1: General scheme of the Smith-Hutton problem

The prescribed velocity field is given by:

$$u(x, y) = 2y(1 - x^2) \quad (6.1)$$

$$v(x, y) = -2x(1 - y^2) \quad (6.2)$$

And the prescribed boundary conditions for the variable ϕ are:

$$\begin{aligned} \phi &= 1 + \tanh(\alpha(2x + 1)), & y = 0; x \in (-1, 0) & \text{(inlet)} \\ \frac{\partial \phi}{\partial y} &= 0, & x = 0; y \in (-1, 0) & \text{(outlet)} \\ \phi &= 1 - \tanh(\alpha), & & \text{(elsewhere)} \end{aligned} \quad (6.3)$$

where $\alpha = 10$.

6.1 Discretization

The spatial discretization is the one explained in section 5.2, and the temporal scheme used is the implicit one, as explained in the same section.

N_x	N_y	δ	Source term
200	100	10^{-9}	0

Table 6.1: Numerical parameters of the Smith-Hutton problem

6.2 Boundary conditions

To apply the boundary conditions to the problem, some modifications on the coefficients defined by equation 5.26 have to be done. The easiest one is for the points in the left, top and right sides of the domain, in which the value of ϕ is defined.

In the bottom it is necessary to distinguish between the inlet and the outlet. A similar approach to that of the left, top and right side is used to determine the coefficients of the points in the inlet. However, in the outlet the only condition is that the derivative of ϕ in the vertical direction is equal to zero. The following reasoning leads to:

$$\frac{\partial \phi}{\partial y} \approx \frac{\phi_N - \phi_P}{\Delta y} = 0 \quad (6.4)$$

$$\phi_P = \phi_N \quad (6.5)$$

The implementation of the boundary conditions in the problem is done with the discretization coefficients listed in table 6.2.

Coefficients	Left, top and right	Inlet (bottom)	Outlet (bottom)
a_E	0	0	0
a_W	0	0	0
a_N	0	0	1
a_S	0	0	0
a_P	1	1	1
b_P	$1 - \tanh(\alpha)$	$1 + \tanh(\alpha(2x + 1))$	0

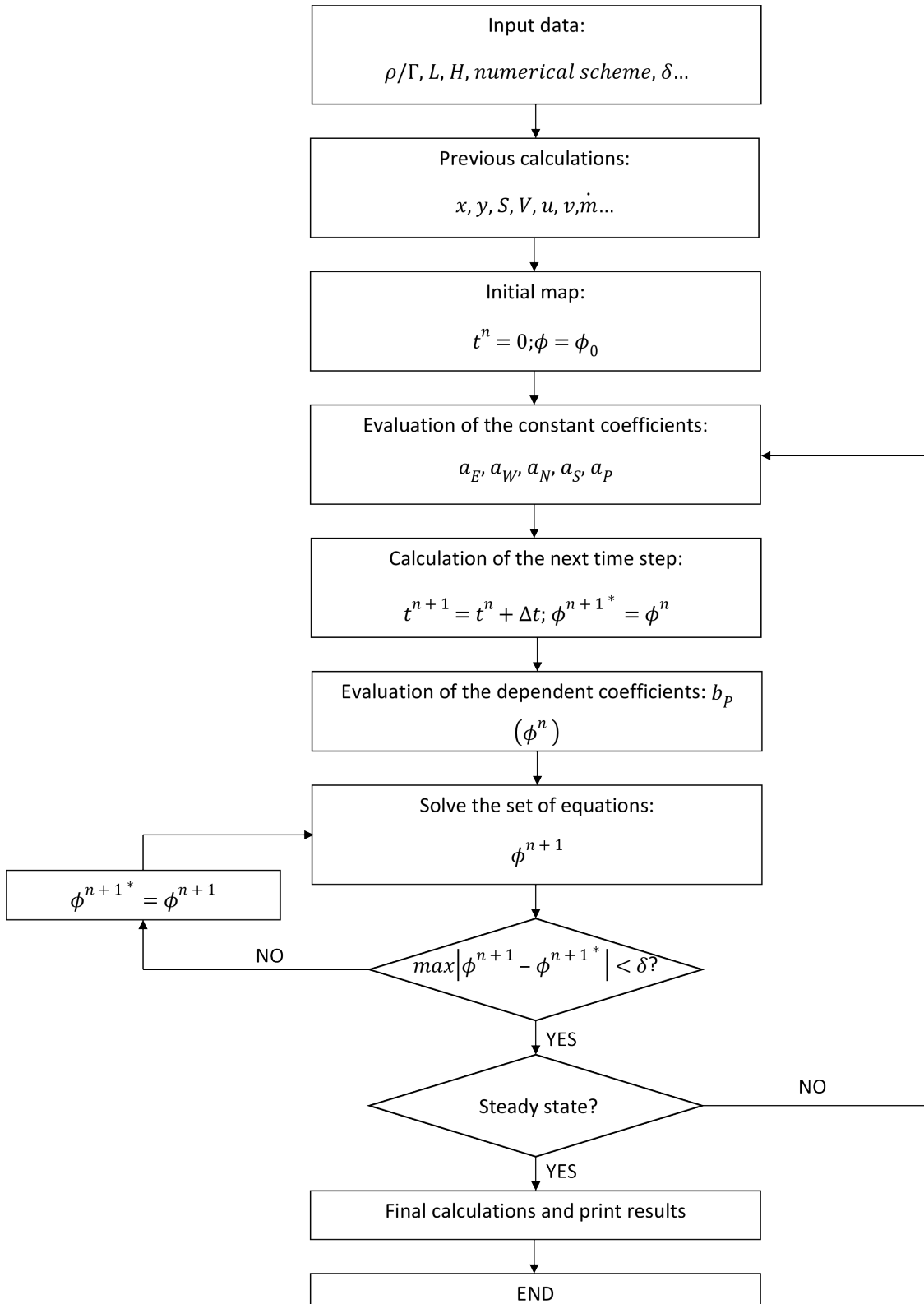
Table 6.2: Discretization coefficients of the boundary points

6.3 Algorithm

The algorithm of resolution is very similar to that used in the four materials problem. The main difference is that in the Smith-Hutton problem the resolution ends when the variable ϕ

Algorithm

reaches a steady state. The schematic algorithm of resolution is displayed below:



6.4 Results

Since the velocity and the dimensions are constant, the parameter ρ/Γ is somehow equivalent to the Péclet number. In order to study the results in different flows, the simulation has been run for three different values of ρ/Γ : 10, 10^3 and 10^6 .

To verify the accuracy of the calculations and the influence of the numerical scheme, the results have to be compared with some reference values. The following figures present the distribution of the variable ϕ in the outlet for all the schemes used and compare them with the benchmark values.

In figure 6.2, when the Péclet number is low, all the methods produce similar results, and there is almost no error compared to the reference values. However, as the Péclet number increases, the error also increases. As it can be seen in figures 6.3 and 6.4, the reference solution displays a sharper distribution than the one obtained in the calculations. The influence of the numerical scheme used is also present in the case of $\rho/\Gamma = 10^3$, when the schemes show slightly different results.

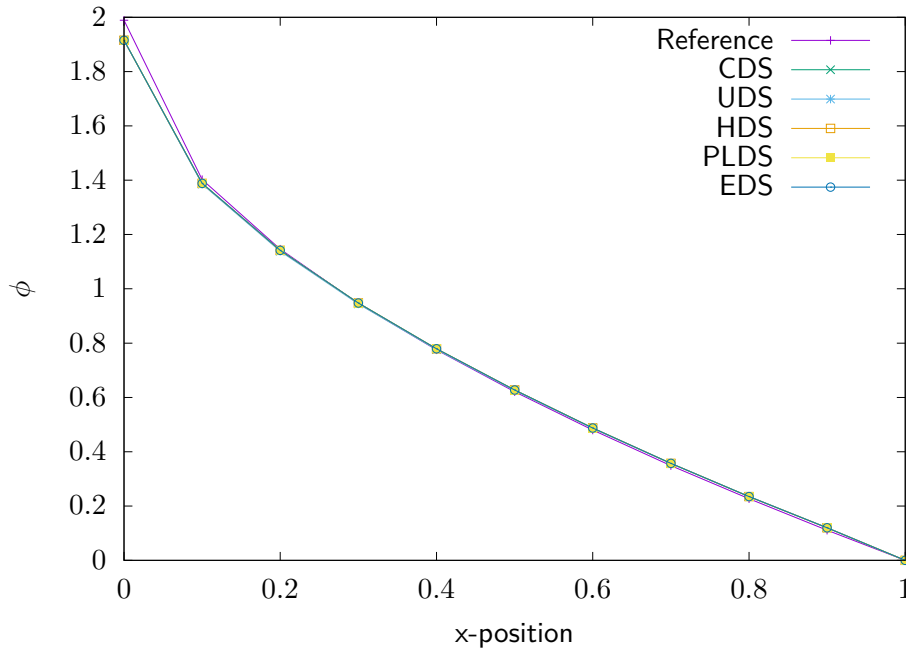


Figure 6.2: Distribution of ϕ at the output for $\rho/\Gamma = 10$

It is important to notice that in the cases $\rho/\Gamma = 10^3$ and $\rho/\Gamma = 10^6$ CDS diverges, and no results are obtained with this method.

Regarding the behaviour of ϕ , for low Péclet numbers, its variation is almost linear, but for high Péclets, it becomes more abrupt, almost a vertical line.

Results

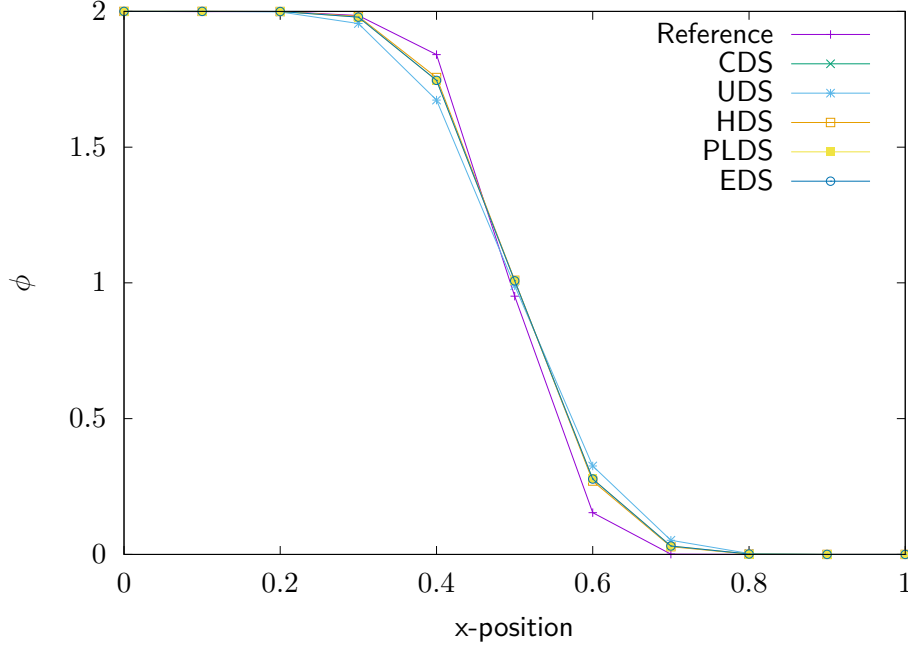


Figure 6.3: Distribution of ϕ at the output for $\rho/\Gamma = 10^3$

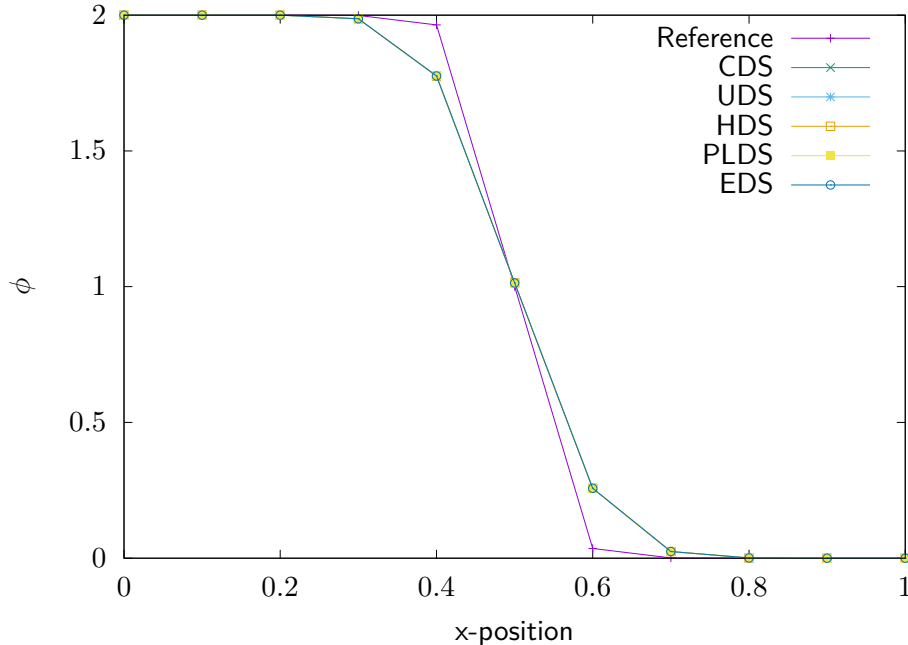


Figure 6.4: Distribution of ϕ at the output for $\rho/\Gamma = 10^6$

Finally, it is interesting to study the variation of the variable ϕ in the whole domain. As it is represented in figure 6.5, for a low Péclet number, since the main transport method is diffusion the variable changes gradually over the domain. But as it increases (figures 6.6 and 6.7), the change is more abrupt, and there is almost no variation except for the centre bottom zone. The distribution of ϕ becomes more symmetrical as the Péclet number increases.

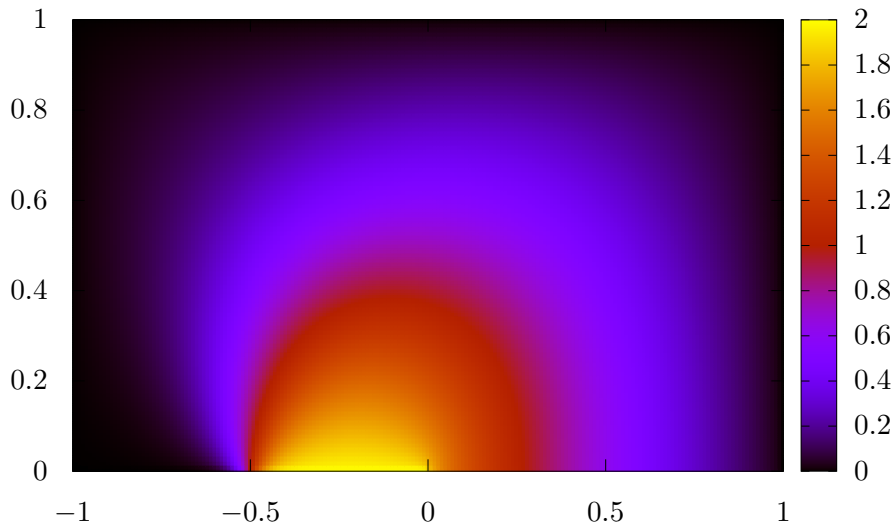


Figure 6.5: Representation of the whole domain for $\rho/\Gamma = 10$ (UDS)

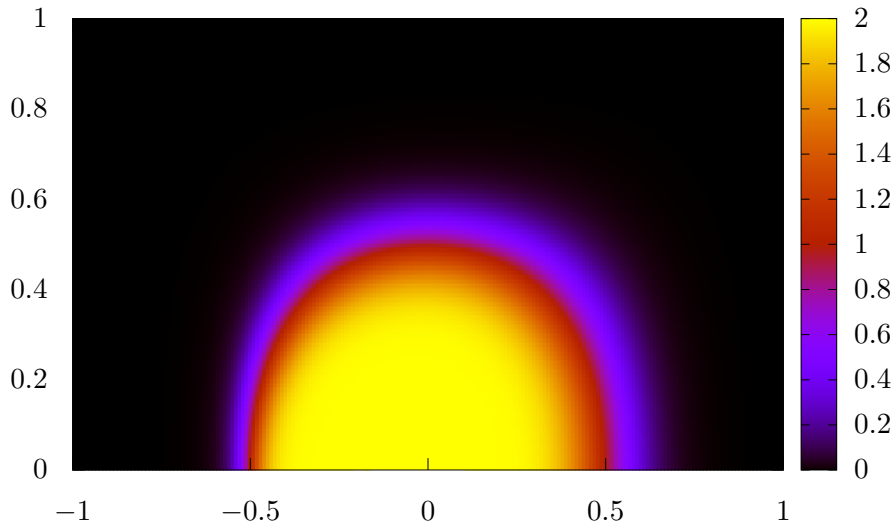


Figure 6.6: Representation of the whole domain for $\rho/\Gamma = 10^3$ (UDS)

As a conclusion, it can be stated that for low Péclet numbers, diffusion dominates over advection, and it tends to uniformly distribute the properties of the inlet to the whole domain. However, as the Péclet number increases advection becomes more important, the influence of the inlet decreases and the velocity field is the one that determines the distribution of the variable ϕ .

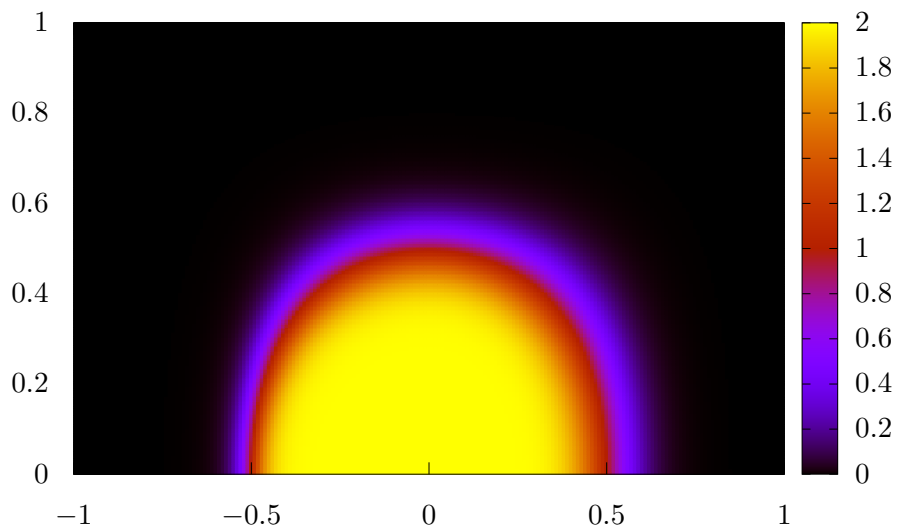


Figure 6.7: Representation of the whole domain for $\rho/\Gamma = 10^6$ (UDS)

Some of the results are plotted in this section, but due to the amount of information, not all of them are in the report. To see more results refer to Attachment A.

7 | Fractional Step Method

The equations to be solved are the conservation of mass and the conservation of momentum:

$$\begin{aligned} \nabla \cdot \vec{v} &= 0 \\ \rho \frac{\partial \vec{v}}{\partial t} + \rho (\vec{v} \cdot \nabla) \vec{v} &= -\nabla p + \mu \nabla^2 \vec{v} \end{aligned} \quad (7.1)$$

7.1 The Helmholtz-Hodge decomposition theorem

According to the Helmholtz-Hodge theorem, it is possible to decompose any vector in a divergence-free vector parallel to the boundary and a gradient field, and this decomposition is unique [5].

To apply the theorem, it is easier to rearrange the Navier-Stokes equation. Assuming constant density and viscosity, the convective and diffusive terms can be grouped together into the single variable $R(\vec{v}) = -\rho(\vec{v} \cdot \nabla) \vec{v} + \mu \nabla^2 \vec{v}$:

$$\rho \frac{\partial \vec{v}}{\partial t} = R(\vec{v}) - \nabla p \quad (7.2)$$

In the numerical integration of equation 7.2 over time the pressure gradient is discretized using an implicit scheme, and the convective term using a central differencing scheme, leading to:

$$\rho \frac{\vec{v}^{n+1} - \vec{v}^n}{\Delta t} = R^{n+\frac{1}{2}}(\vec{v}) - \nabla p^{n+1} \quad (7.3)$$

where $t^{n+1/2}$ is the instant of time between t^n and t^{n+1} . To evaluate the convection-diffusion term, the Adams-Bashforth second-order scheme is used:

$$R^{n+\frac{1}{2}}(\vec{v}) \approx \frac{3}{2}R(\vec{v}^n) - \frac{1}{2}R(\vec{v}^{n-1}) \quad (7.4)$$

As an application of the Helmholtz-Hodge theorem, the intermediate velocity is defined as the sum of a divergence-free vector, the velocity, and the gradient of a scalar field, the pressure:

$$\vec{v}^P = \vec{v}^{n+1} + \nabla \tilde{p} = \vec{v}^{n+1} + \frac{\Delta t}{\rho} p^{n+1} \quad (7.5)$$

Introducing this expression to the integrated equation:

$$\rho \frac{\vec{v}^P - \vec{v}^n}{\Delta t} = R^{n+\frac{1}{2}}(\vec{v}) \quad (7.6)$$

And finally, applying the divergence to the expression of the intermediate velocity \vec{v}^P 7.5, the Poisson equation is obtained:

$$\nabla \cdot \vec{v} = \frac{\Delta t}{\rho} \nabla^2 p \quad (7.7)$$

7.2 Fractional Step Method algorithm

With all these expressions the fractional step method (FSM) can be finally implemented, following the next scheme:

1. Evaluate $R^{n+\frac{1}{2}}(\vec{v})$.
2. Calculate the intermediate velocity with equation 7.6.
3. Calculate the pressure p^{n+1} from the Poisson equation 7.7 using a linear solver.
4. Apply the pressure correction given by 7.5 to calculate the velocity at the next time step.

However, the FSM can be problematic if the mesh of the problem is not correctly implemented. To avoid having unrealistic solutions, it is important to use staggered meshes or collocated meshes. The discretization of the domain as well as a further explanation of the described steps are going to be developed in the following sections.

7.3 Discretization

To avoid convergence problems or incorrect solutions (checkerboard problem [6]), staggered meshes are used. As shown in figure 7.1, in a two-dimensional case there are 3 control volumes, one for each variable: p_P , u_P and v_P . They are coloured in black, red and green respectively. The black dots are the nodes in which the pressure is calculated, the red arrows are the nodes of the horizontal velocity, and the green arrows are the nodes of the vertical velocity.

7.3.1 Intermediate velocity discretization

First of all, it is necessary to discretize the expression of $R(\vec{v})$ of the equation 7.2:

$$R(\vec{v}) = -\rho(\vec{v} \cdot \nabla)\vec{v} + \mu\nabla^2\vec{v} \quad (7.8)$$

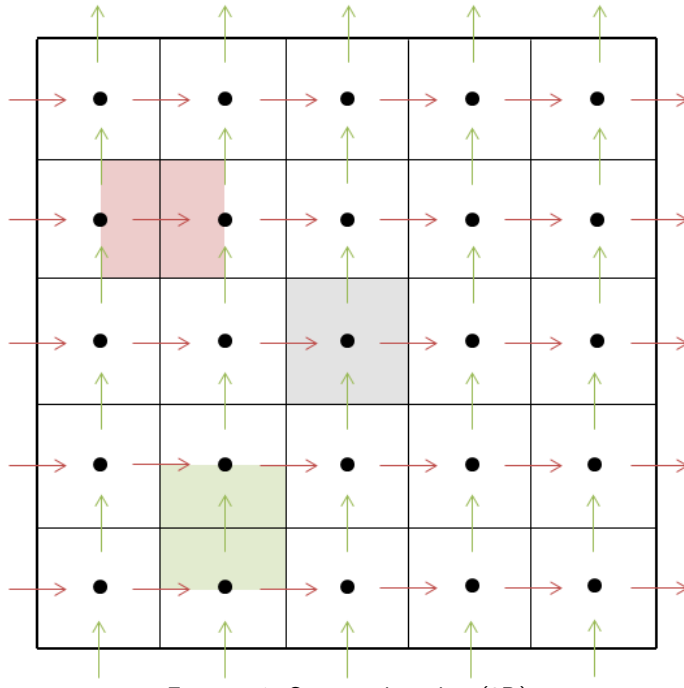


Figure 7.1: Staggered meshes (2D)

This variable is a vector, so it has to be discretized in two directions: one for the horizontal velocity u and another one for the vertical velocity v . Integrating the expression over the control volume of the horizontal velocity staggered mesh in the horizontal direction:

$$\int_{\Omega_x} R(u) d\Omega_x = - \int_{\Omega_x} (\rho \vec{v} \cdot \nabla) u d\Omega_x + \int_{\Omega_x} \mu \nabla^2 u d\Omega_x \quad (7.9)$$

Applying the Gauss theorem:

$$R(u) V_P = - \int_{\partial \Omega_x} (\rho \vec{v}) u \cdot \vec{n} dS + \int_{\partial \Omega_x} \mu \nabla u \cdot \vec{n} dS \quad (7.10)$$

The final integration of $R(\vec{v})$ in the horizontal direction results as:

$$\begin{aligned} R(u) V_P = & \left[\mu_e \frac{u_E - u_P}{d_{EP}} A_e + \mu_n \frac{u_N - u_P}{d_{NP}} A_n - \mu_w \frac{u_P - u_W}{d_{WP}} A_w - \mu_s \frac{u_P - u_S}{d_{SP}} A_s \right] \\ & - [(\rho u)_e u_e A_e + (\rho v)_n u_n A_n - (\rho u)_w u_w A_w - (\rho v)_s u_s A_s] \end{aligned} \quad (7.11)$$

The same approach is used in the vertical direction, obtaining the following expression:

$$\begin{aligned} R(v) V_P = & \left[\mu_e \frac{v_E - v_P}{d_{EP}} A_e + \mu_n \frac{v_N - v_P}{d_{NP}} A_n - \mu_w \frac{v_P - v_W}{d_{WP}} A_w - \mu_s \frac{v_P - v_S}{d_{SP}} A_s \right] \\ & - [(\rho u)_e v_e A_e + (\rho v)_n v_n A_n - (\rho u)_w v_w A_w - (\rho v)_s v_s A_s] \end{aligned} \quad (7.12)$$

The main problem of these expressions is the evaluation of the velocities and the mass flows in the faces of the control volume. To calculate the velocities in the faces some of the numerical schemes previously discussed are used: CDS, UDS... In the case of the mass flows per surface unit, the staggered meshes have to be taken into account:

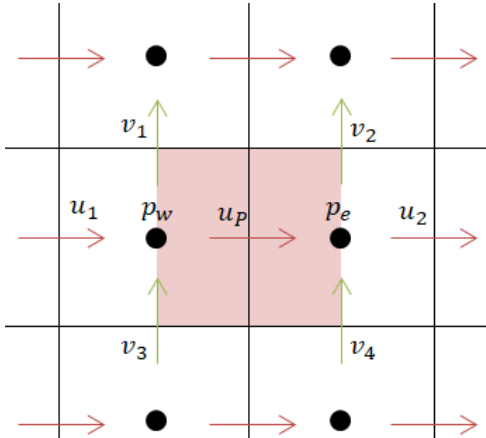


Figure 7.2: Control volume of the horizontal velocity

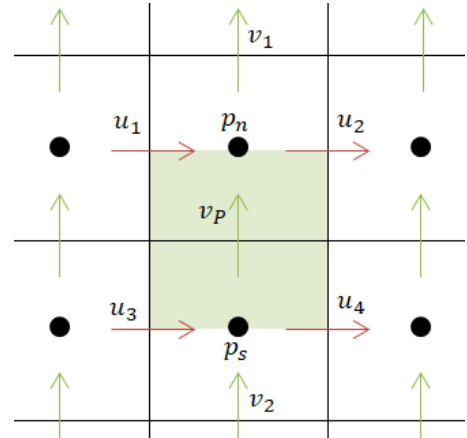


Figure 7.3: Control volume of the vertical velocity

- The calculation of the mass flow per surface unit in the control volume of the horizontal velocity 7.2 is simple in the case of the horizontal mass flows:

$$(\rho u)_e = \frac{\rho u_P + \rho u_2}{2} \quad (7.13)$$

$$(\rho u)_w = \frac{\rho u_1 + \rho u_P}{2} \quad (7.14)$$

But the vertical flows are somehow more difficult:

$$(\rho v)_n = \frac{\rho v_1 + \rho v_2}{2} \quad (7.15)$$

$$(\rho v)_s = \frac{\rho v_3 + \rho v_4}{2} \quad (7.16)$$

- The calculation of the mass flow per surface unit in the control volume of the vertical velocity 7.3 is similar to that of the horizontal velocity. Starting with the horizontal flows:

$$(\rho u)_e = \frac{\rho u_2 + \rho u_4}{2} \quad (7.17)$$

$$(\rho u)_w = \frac{\rho u_1 + \rho u_3}{2} \quad (7.18)$$

And the vertical ones:

$$(\rho v)_n = \frac{\rho v_1 + \rho v_P}{2} \quad (7.19)$$

$$(\rho v)_s = \frac{\rho v_P + \rho v_2}{2} \quad (7.20)$$

Once the value of $R(\vec{v})$ is calculated using the expressions developed above and the Adams-Bashforth scheme 7.4, the intermediate velocity can be computed rearranging the equation 7.6:

$$\vec{v}^P = \vec{v}^n + \frac{\Delta t}{\rho} R^{n+\frac{1}{2}}(\vec{v}) \quad (7.21)$$

7.3.2 Pressure discretization

The next step is to obtain the pressure in the next time step with the Poisson equation. Knowing the space discretization of the domain, the discretized Poisson equation can be calculated. Integrating the expression 7.7 over the domain and applying the divergence theorem, the following expression is obtained:

$$\frac{p_E^{n+1} - p_P^{n+1}}{d_{EP}} A_e + \frac{p_N^{n+1} - p_P^{n+1}}{d_{NP}} A_n - \frac{p_P^{n+1} - p_W^{n+1}}{d_{WP}} A_w - \frac{p_P^{n+1} - p_S^{n+1}}{d_{SP}} A_s = \frac{1}{\Delta t} \left[(\rho u^P)_e A_e + (\rho v^P)_n A_n - (\rho u^P)_w A_w - (\rho v^P)_s A_s \right] \quad (7.22)$$

Rewriting the equation using discretization coefficients:

$$a_P p_P^{n+1} = a_E p_E^{n+1} + a_W p_W^{n+1} + a_N p_N^{n+1} + a_S p_S^{n+1} + b_P \quad (7.23)$$

where

$$a_P = a_E + a_W + a_N + a_S \quad (7.24)$$

$$a_E = \frac{A_e}{d_{EP}} \quad (7.25)$$

$$a_W = \frac{A_w}{d_{WP}} \quad (7.26)$$

$$a_N = \frac{A_n}{d_{NP}} \quad (7.27)$$

$$a_S = \frac{A_s}{d_{SP}} \quad (7.28)$$

$$b_P = -\frac{1}{\Delta t} \left[(\rho u^P)_e A_e + (\rho v^P)_n A_n - (\rho u^P)_w A_w - (\rho v^P)_s A_s \right] \quad (7.29)$$

7.3.3 Velocity discretization

With equation 7.5 the horizontal and vertical velocities at the next time step can be calculated:

$$u_P^{n+1} = u_P^P - \frac{\Delta t}{\rho} \frac{p_e^{n+1} - p_w^{n+1}}{d_{ew}} \quad (7.30)$$

$$v_P^{n+1} = v_P^P - \frac{\Delta t}{\rho} \frac{p_n^{n+1} - p_s^{n+1}}{d_{ns}} \quad (7.31)$$

7.4 Time step

The fractional step method is an explicit method. In order to obtain accuracy in the results, the time step has to be correctly chosen. To do so, it is recalculated in each iteration of the algorithm using a Courant-Friedrich-Levy (CFL) condition. Two time steps are defined, one of them depends on the convective term and the other one on the diffusive term:

$$\Delta t_c = \min \left(0.35 \frac{\Delta x}{|v|} \right) \quad (7.32)$$

$$\Delta t_d = \min \left(0.20 \frac{\rho (\Delta x)^2}{\mu} \right) \quad (7.33)$$

If the mesh, the density and the viscosity are constant, the time step defined by the diffusive term is constant, so it only has to be calculated at the beginning of the simulation, as it does not depend on the velocity. But the time step given by the convective term changes with each iteration. The final time step that is used is the smallest one:

$$\Delta t = \min (\Delta t_c, \Delta t_d) \quad (7.34)$$

8 | Driven cavity problem

The driven cavity problem consists in a two-dimensional cavity with an incompressible fluid. The upper wall of the cavity moves at a given velocity, as shown in figure 8.1. The aim of the problem is to obtain the distribution of velocities inside the cavity.

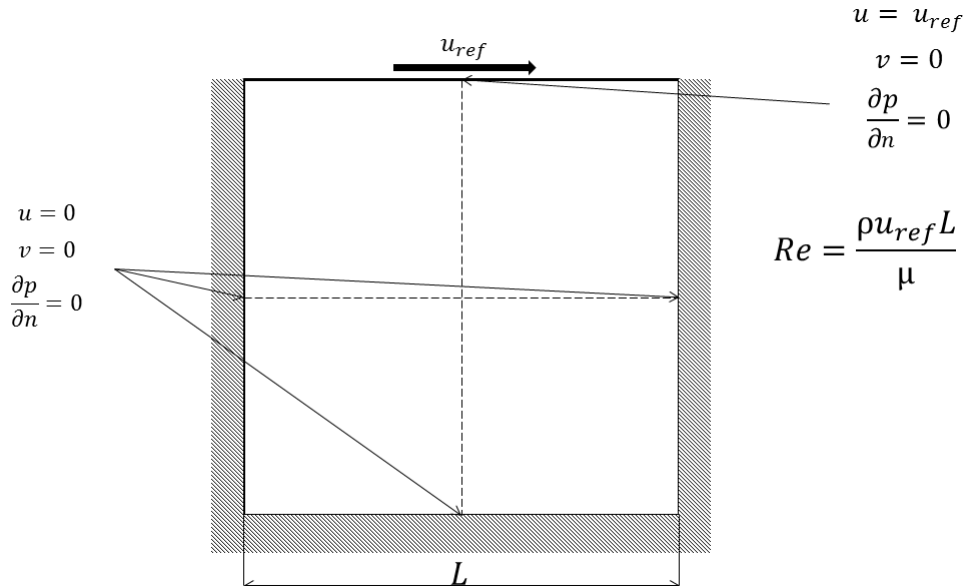


Figure 8.1: General scheme of the driven cavity problem. Extracted from [6]

8.1 Discretization

The domain is discretized, as explained in section 7.3, using the staggered meshes. To do so, the volume is divided using a Cartesian grid, with the following characteristics:

N	M	L	ρ	u_{ref}	μ	$Numerical\ scheme$	δ
112	112	1	1	1	$\frac{1}{Re}$	CDS	10^{-5}

Table 8.1: Numerical parameters of the driven cavity problem

The length of the cavity L , the density ρ , the velocity u_{ref} and the viscosity μ are chosen in order to have a non-dimensional problem.

8.2 Boundary conditions

It is necessary to impose the conditions defined by figure 8.1. There are two types of conditions: the prescribed velocity, and the boundary layer conditions. The last ones are defined by assuming that the pressure gradient normal to the wall is 0. For example, in the left wall:

$$\frac{\partial p}{\partial x} \approx \frac{p_E - p_P}{\Delta x} = 0 \quad (8.1)$$

$$p_P = p_E \quad (8.2)$$

These boundary layer conditions modify the discretization coefficients in the boundary nodes. The coefficients are listed in table 8.2.

Coefficients	Top	Bottom	Left	Right
a_E	1	0	1	0
a_W	0	0	0	1
a_N	0	1	0	0
a_S	0	0	0	0
a_P	1	1	1	1

Table 8.2: Discretization coefficients in the boundary

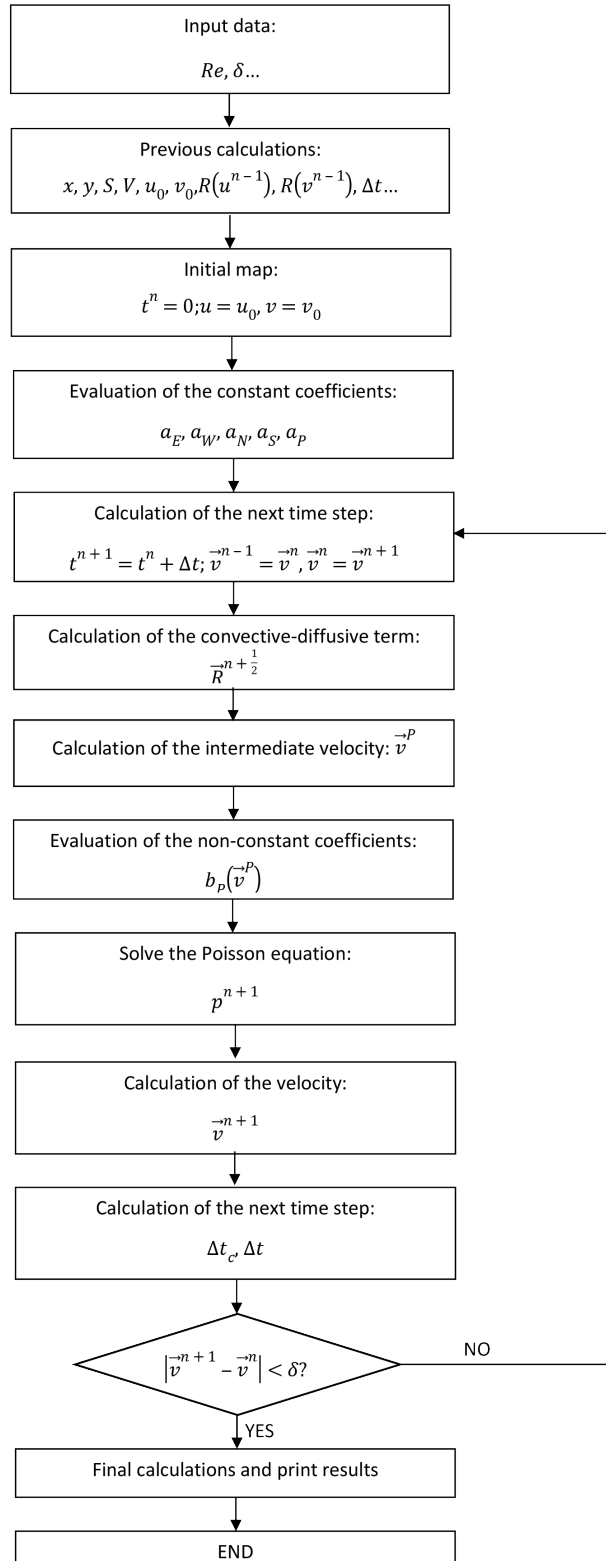
The condition of prescribed velocity in the walls is achieved with the following conditions:

- $R(\vec{v}) = 0$ in the top
- $R(\vec{v}) = 0$ in the bottom wall
- $R(\vec{v}) = 0$ in the left wall
- $R(\vec{v}) = 0$ in the right wall

And the prescribed velocities are:

- $u = u_{ref}, v = 0$ in the top
- $u = 0, v = 0$ in the bottom wall
- $u = 0, v = 0$ in the left wall
- $u = 0, v = 0$ in the right wall

8.3 Algorithm



The simulation of the driven cavity problem ends when it reaches a steady state.

8.4 Results

In order to study the behaviour of the driven cavity problem in different ranges of flow, the simulation has been tested for $Re = 100, 400, 1000, 3200, 5000, 7500$ and 10000 . However not all cases are in the report; to see more results refer to Attachment A.

Figures 8.2 and 8.3 are a comparison between the obtained results and the reference ones for the velocities in the central planes. In both vertical and horizontal velocities, the best results are obtained for $Re = 1000$. For low Reynolds the difference is slightly higher, but the results are still accurate. In the case of $Re = 3200$ there is a point that presents a big error, but since it does not follow the distribution of the others it may be a typographical error. However, as the Reynolds increases, the error increases as well. In the cases of $Re \geq 5000$, the results are rather different from the expected ones. Since these are high Reynolds, they may have not reached a steady state because they are turbulent.

As for the distribution of velocities, it can be seen that as the Reynolds increases the variation becomes sharper, especially near the walls, where the gradient of velocities is higher. For the horizontal velocities, the shape of the curve is very different for lower and higher Reynolds.

Looking at the variation of the horizontal velocity in the whole domain (figure 8.4), for lower Reynolds, there is only a small movement in the top of the cavity. But as the Re increases, more fluid becomes involved with the clockwise rotation, increasing its radius. For $Re = 10000$, the distribution shows that only the outer radius of the cavity rotates. However, these results may not be realistic due to the error obtained at high Reynolds.

For the vertical velocities (figure 8.5) the behaviour is similar to that of the horizontal velocities. For low Re, there is only velocity in the top of the vertical walls. However, as the Re increases, the region with vertical velocity also increases, showing again the distribution of a clockwise rotation. The gradient of velocities in the right wall is stronger for higher Reynolds numbers. In the case of $Re = 10000$ the distribution shows that the region with vertical velocity stretches, but these results may not be accurate.

As a conclusion, for lower Reynolds numbers, viscosity only allows a small movement in the upper region of the cavity. This is the case of $Re = 100$. But for higher Re, inertial forces become more important and the behaviour of the flow is completely different. The fluid starts to rotate around the centre of the cavity. As the Re increases, the motion becomes more complex and other small vortices appear in the sides of the cavity, as it can be seen in figure 8.6.

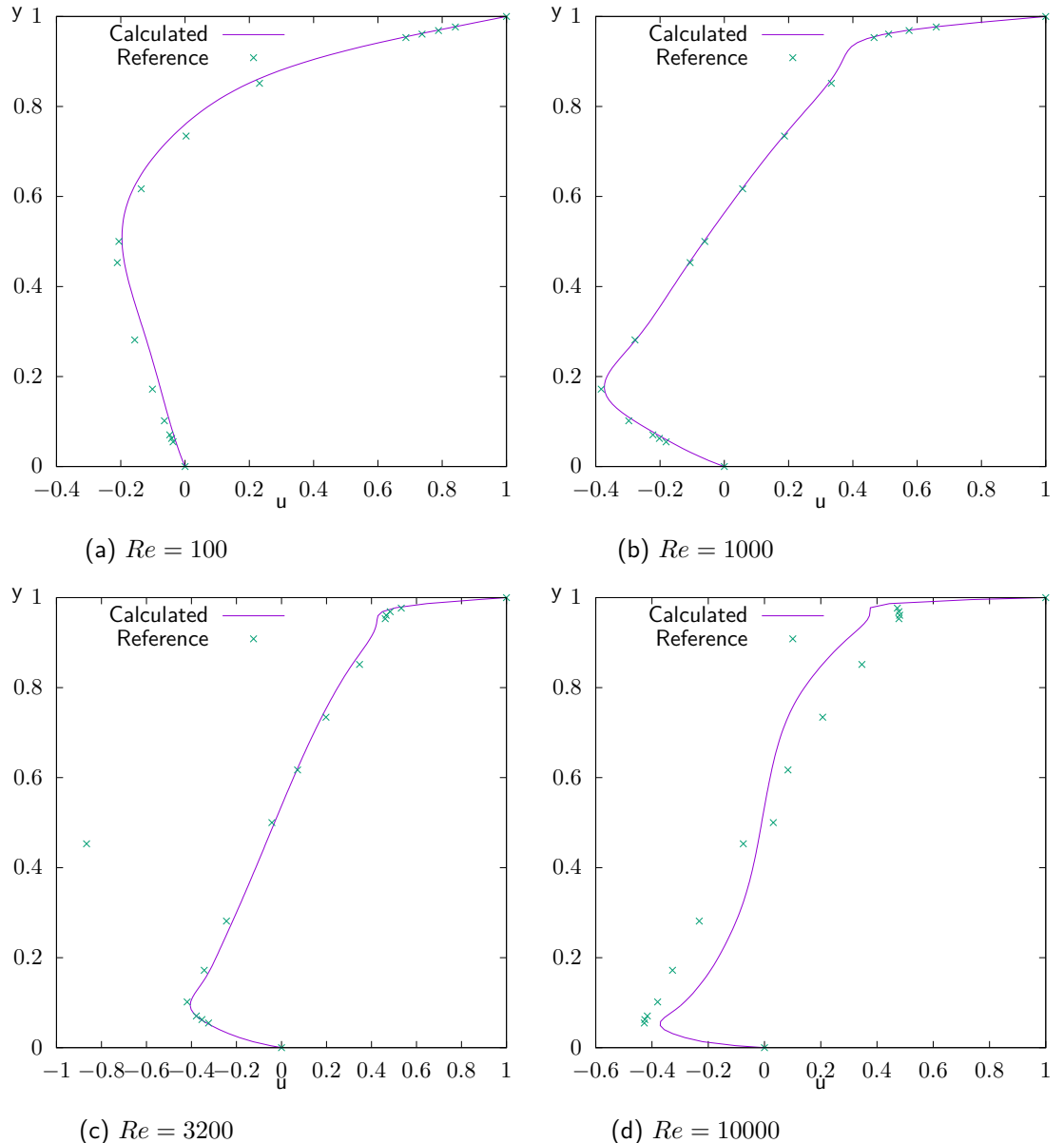


Figure 8.2: Comparison between the reference solution and the calculated one of the horizontal velocity along the vertical line in the geometric centre of the cavity [7]

Results

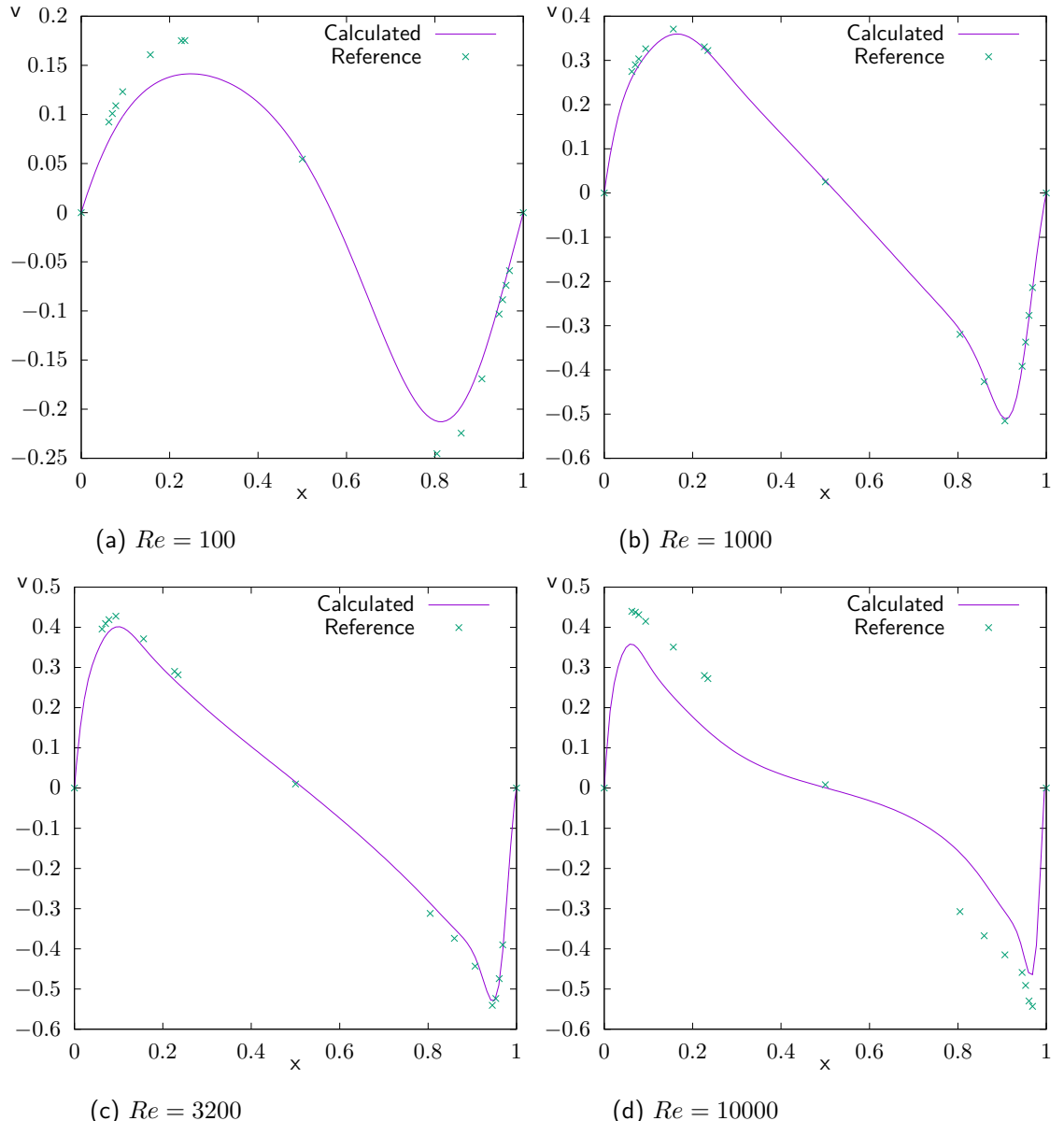


Figure 8.3: Comparison between the reference solution and the calculated one of the vertical velocity along the horizontal line in the geometric centre of the cavity [7]

Results

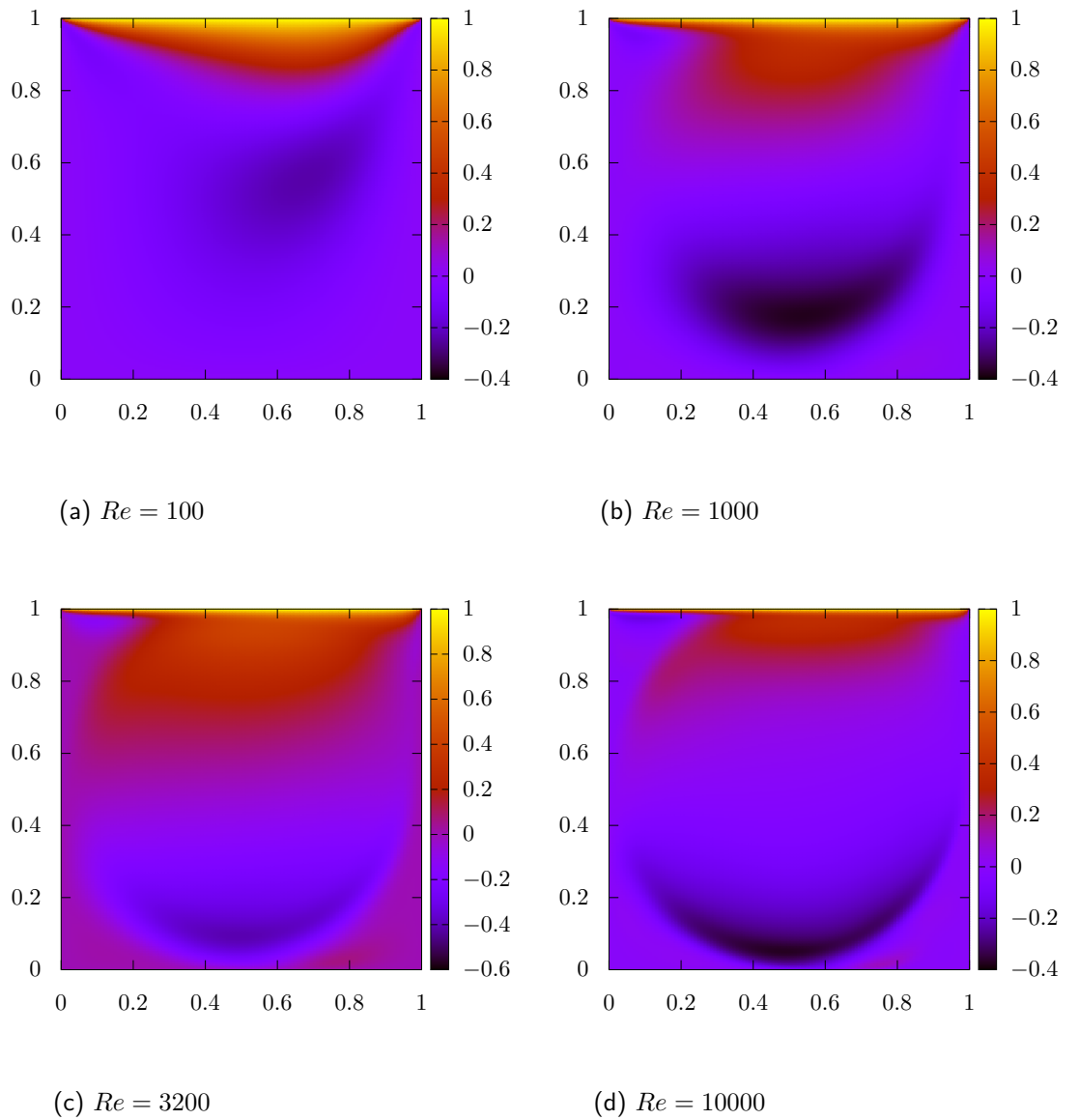


Figure 8.4: Horizontal velocity in the cavity

Results

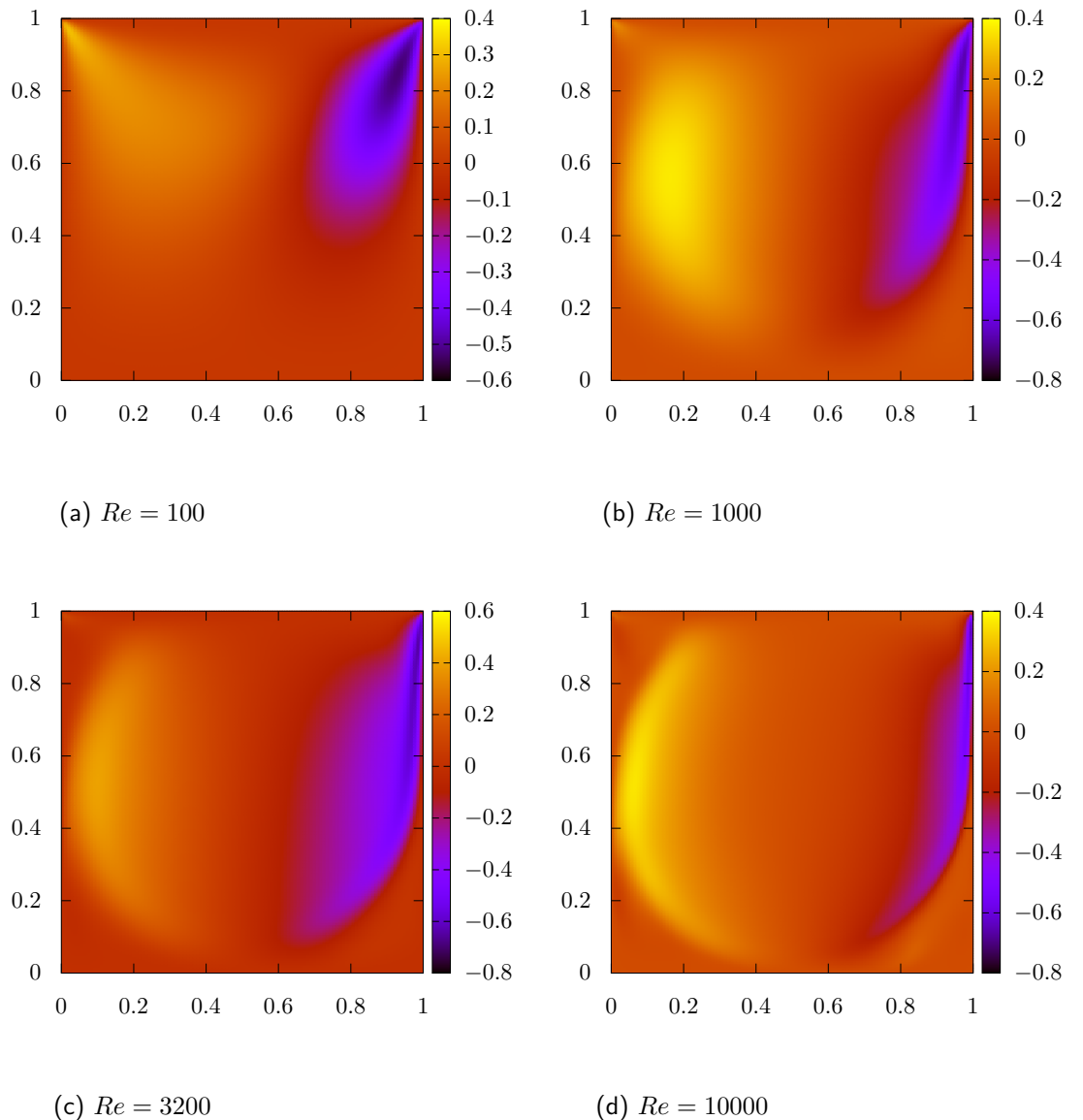


Figure 8.5: Vertical velocity in the cavity

Results

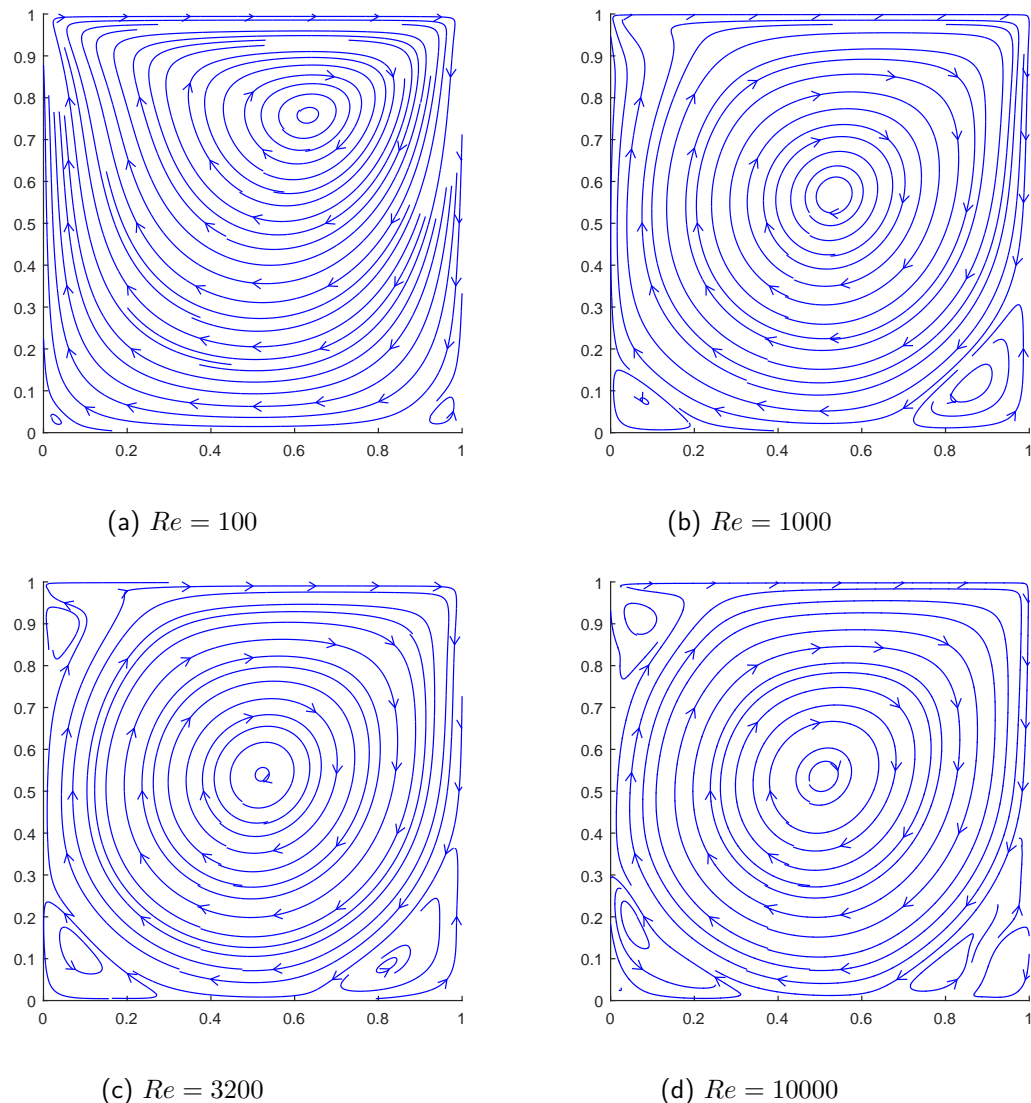


Figure 8.6: Streamlines of the flow inside the cavity

9 | Differentially heated cavity

The differentially heated cavity problem or buoyancy-driven cavity problem is a two dimensional problem based on free convection. It comprises a cavity with the vertical walls at different temperatures and adiabatic horizontal walls [8, 9]. The difference of temperatures between the two vertical walls causes convection.

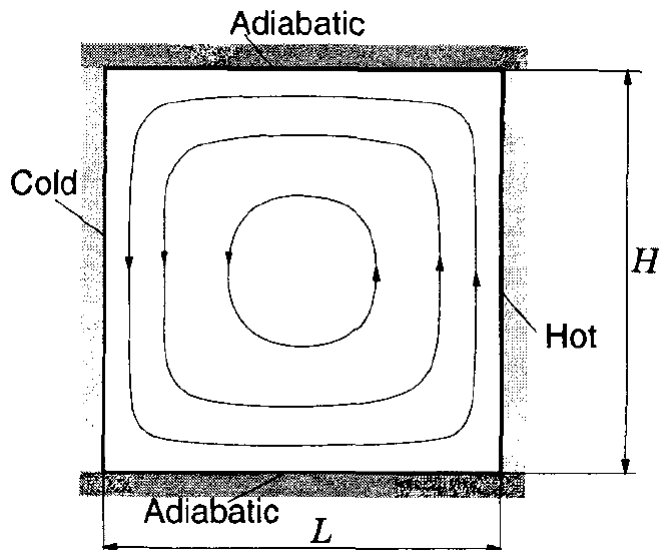


Figure 9.1: General scheme of the differentially heated problem. Extracted from [1]

9.1 Natural convection

The equations that are going to be discretized are the two-dimensional equations of mass, momentum and energy for a Newtonian fluid with constant properties. However, some approximations have to be done for the momentum equation:

$$\rho_0 \frac{\partial \vec{v}}{\partial t} + \rho_0 (\vec{v} \cdot \nabla) \vec{v} = -\nabla p + \mu \nabla^2 \vec{v} + \rho \vec{g} \quad (9.1)$$

As it can be seen, mass forces have been added to the momentum equation, because in natural convection gravity is not negligible. Another important remark is that the fluid is considered

incompressible, but this approximation is not applied in the gravitational term, because it is this term that causes the flow. However, as a simplification, the Boussinesq approximation is applied [3, 10]:

$$\rho = \rho_0 (1 - \beta (T - T_0)) \quad (9.2)$$

where β is the volumetric thermal expansion coefficient, a thermodynamic property that measures the variation of the density as a function of the temperature at a constant pressure. Introducing the Boussinesq approximation in the momentum equation, the final equations for natural convection are:

$$\nabla \cdot \vec{v} = 0 \quad (9.3)$$

$$\rho_0 \frac{\partial \vec{v}}{\partial t} + \rho_0 (\vec{v} \cdot \nabla) \vec{v} = -\nabla p_d + \mu \nabla^2 \vec{v} - \rho_0 \beta (T - T_0) \vec{g} \quad (9.4)$$

$$\rho c_p \left(\frac{\partial T}{\partial t} + \vec{v} \cdot \nabla T \right) = \lambda \nabla^2 T \quad (9.5)$$

9.1.1 Non-dimensional equations

In order to have a simpler analysis, it is convenient to use non-dimensional variables. Depending on the problem, they can be defined by several different ways. In this section, taking into account the most important variables of a free convection problem, the dimensionless variables are defined as it is expressed below:

$$\vec{x}^* = \frac{\vec{x}}{L} \quad (9.6)$$

$$\vec{v}^* = \frac{\vec{v}}{\frac{\lambda}{\rho L c_P}} \quad (9.7)$$

$$t^* = \frac{t}{\frac{\rho L^2 c_P}{\lambda}} \quad (9.8)$$

$$p^* = \frac{p}{\frac{1}{\rho} \left(\frac{\lambda}{c_P L} \right)^2} \quad (9.9)$$

$$T^* = \frac{T - T_{cold}}{T_{hot} - T_{cold}} \quad (9.10)$$

Inserting these expressions in the equations 9.3, 9.4 and 9.5, the non-dimensional equations for natural convection are obtained. In order to simplify the notation, the indexes * have been removed, but the variables that are represented in the following section are the dimensionless ones.

$$\nabla \cdot \vec{v} = 0 \quad (9.11)$$

$$\frac{\partial \vec{v}}{\partial t} + (\vec{v} \cdot \nabla) \vec{v} = -\nabla p + Pr \nabla^2 \vec{v} - Pr Ra T \vec{u}_g \quad (9.12)$$

$$\frac{\partial T}{\partial t} + \vec{v} \cdot \nabla T = \nabla^2 T \quad (9.13)$$

The dimensionless numbers that appear are the Prandtl and Rayleigh numbers, defined as:

$$Pr \equiv \frac{c_P \mu}{\lambda} \quad (9.14)$$

$$Ra \equiv \frac{\rho^2 g \beta \Delta T L^3 c_P}{\mu \lambda} \quad (9.15)$$

where $\Delta T = T_{hot} - T_{cold}$.

9.2 Application of the fractional step method

The resolution of this problem can be done using the fractional step method described in chapter 7. In the case of the momentum equation its resolution is done as it is explained in the mentioned section. But the expression of the equation is slightly different. Rewriting the momentum equation as it was done:

$$\frac{\partial \vec{v}}{\partial t} = R(\vec{v}) - \nabla p \quad (9.16)$$

where

$$R(\vec{v}) = -(\vec{v} \cdot \nabla) \vec{v} + Pr \nabla^2 \vec{v} - Pr Ra T \vec{u}_g \quad (9.17)$$

The other important issue is the introduction of the energy equation. It has to be discretized according to the fractional step method. As it can be seen, this case is very similar to the previously studied Smith-Hutton problem, since the velocity field is "known" (calculated by other means) and the unknown is a scalar. Therefore, an implicit scheme is going to be used for the temporal integration:

$$\frac{T^{n+1} - T^n}{\Delta t} = [-\vec{v} \cdot \nabla T + \nabla^2 T]^{n+1} \quad (9.18)$$

9.3 Discretization

The spatial discretization of the domain is the one described by the figure 7.1: a Cartesian grid with a staggered mesh.

The discretization of the momentum equation is very similar to that described in the fractional step method chapter but adding the gravity term in the case of the vertical equation:

$$R(u) V_P = \left[Pr_e \frac{u_E - u_P}{d_{EP}} A_e + Pr_n \frac{u_N - u_P}{d_{NP}} A_n - Pr_w \frac{u_P - u_W}{d_{WP}} A_w - Pr_s \frac{u_P - u_S}{d_{SP}} A_s \right] \\ - [(u)_e u_e A_e + (v)_n u_n A_n - (u)_w u_w A_w - (v)_s u_s A_s] \quad (9.19)$$

$$R(v) V_P = \left[Pr_e \frac{v_E - v_P}{d_{EP}} A_e + Pr_n \frac{v_N - v_P}{d_{NP}} A_n - Pr_w \frac{v_P - v_W}{d_{WP}} A_w - Pr_s \frac{v_P - v_S}{d_{SP}} A_s \right] - [(u)_e v_e A_e + (v)_n v_n A_n - (u)_w v_w A_w - (v)_s v_s A_s] + Pr Ra T V_P \quad (9.20)$$

In the case of the energy equation a similar approach is used. Temperature, like pressure, is evaluated in the nodes, not in the faces like the velocities. The integration of the terms of the equations starts with the Gauss Theorem:

$$\int_{\Omega} \vec{v} \nabla T d\Omega = \int_{\partial\Omega} \vec{v} \cdot \vec{n} T dS \approx (u)_e T_e A_e + (v)_n T_n A_n - (u)_w T_w A_w - (v)_s T_s A_s \quad (9.21)$$

$$\int_{\Omega} \nabla^2 T d\Omega = \int_{\partial\Omega} \nabla T dS \approx \frac{T_E - T_P}{d_{PE}} A_e + \frac{T_N - T_P}{d_{PN}} A_n - \frac{T_P - T_W}{d_{PW}} A_w - \frac{T_P - T_S}{d_{PS}} A_s \quad (9.22)$$

The temperature in the faces is evaluated using the central differencing scheme, as it was done for the velocities.

The final discretized equation for the temperature can be expressed as:

$$a_P T_P = a_E T_E + a_W T_W + a_N T_N + a_S T_S + b_p \quad (9.23)$$

where the discretized coefficients are the same discussed in section 5.3 for a central differencing scheme.

9.4 Boundary conditions

Since the cavity is all surrounded by walls, the boundary velocities are:

- $\vec{v} = 0$ in the top wall
- $\vec{v} = 0$ in the bottom wall
- $\vec{v} = 0$ in the left wall
- $\vec{v} = 0$ in the right wall

In the case of the temperature, they are determined in the right and left walls. Taking into account the expression of T in the equation 9.10:

- $T = 1$ in the left wall
- $T = 0$ in the right wall

In the top and bottom walls the only condition is that they are adiabatic. This condition can also be expressed as:

$$\frac{\partial T}{\partial y} \approx \frac{T_P - T_S}{d_{PS}} = 0 \quad (9.24)$$

$$T_P = T_S \quad (9.25)$$

As a consequence, the discretized coefficients of the boundary nodes have the values listed in table 9.1.

Coefficients	Left	Right	Top	Bottom
a_E	0	0	0	0
a_W	0	0	0	0
a_N	0	0	0	1
a_S	0	0	1	0
a_P	1	1	1	1
b_P	0	1	0	0

Table 9.1: Discretization coefficients of the boundary temperature nodes

9.5 Nusselt number

In the differentially heated cavity, the motion occurs due to the convective transfer. In other words, the temperature gradient is the important issue in this problem, so it would be useful to calculate it. The local heat flux in a horizontal direction at any point in the cavity [9]:

$$Q(x, y) = uT - \frac{\partial T}{\partial x} \quad (9.26)$$

The Nusselt number is a non-dimensional parameter that can be seen as the dimensionless temperature gradient. It provides a measure of the convection heat at a surface [3]. The local Nusselt number gives the heat flow through any vertical line:

$$Nu_x = \int_0^1 Q(x, y) dy \quad (9.27)$$

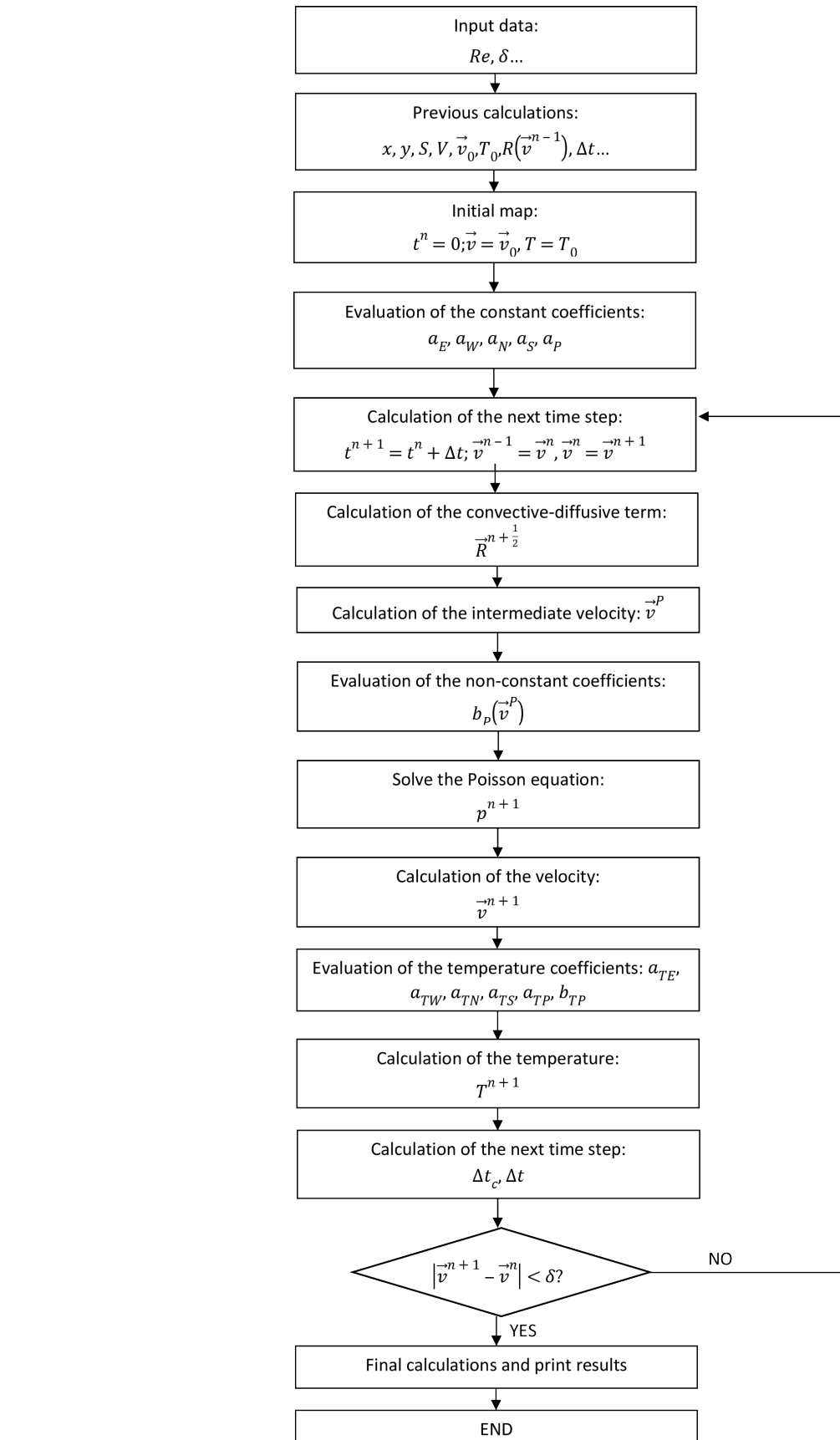
Another useful value is the average Nusselt number of the whole cavity:

$$\overline{Nu} = \int_0^1 Nu_x dx \quad (9.28)$$

9.6 Algorithm

The algorithm used to calculate this problem is very similar to that of the driven cavity problem, but adding the resolution of the temperature. As in the previous program, the simulation ends when the cavity reaches a steady state.

Algorithm



9.7 Results

In order to provide different ranges of solutions, the code has been tested for different Rayleigh numbers. The parameters of the simulations are listed in table 9.2.

N	M	L	H	Pr	δ
50	50	1	1	0.71	10^{-4}

Table 9.2: Numerical parameters of the differentially heated cavity problem

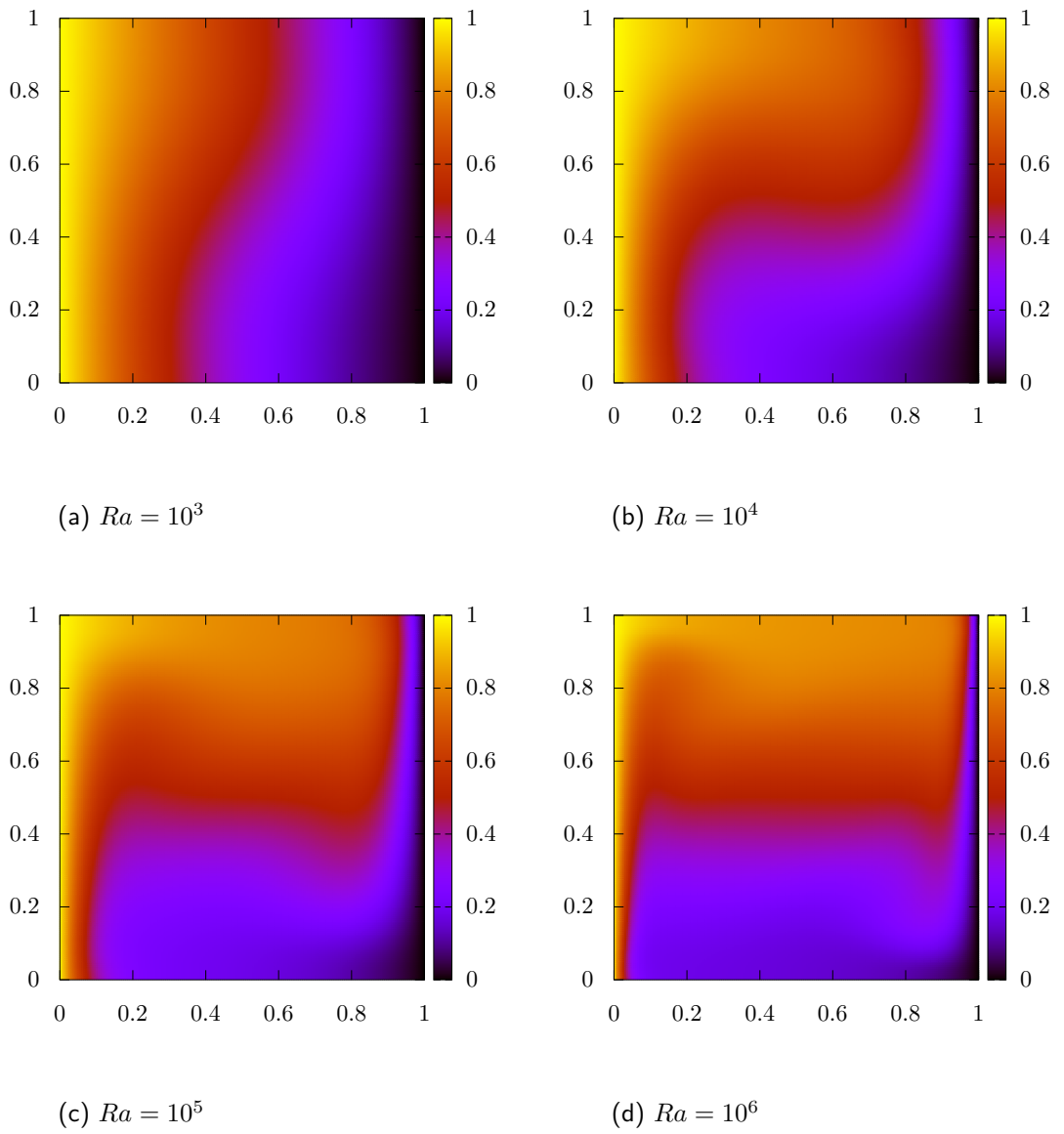


Figure 9.2: Contour plots of the temperature

Results

In the temperature distribution (figure 9.2), there is a curve of the hot fluid (left wall) to the right in the top, whereas in the bottom the temperature decreases faster. This is the expected behaviour because higher temperatures mean lower densities, so the hot fluid tends to go to the top. At low Ra, the temperature distribution is almost linear, like in conduction. But as Ra increases, the mentioned curve becomes more pronounced, until the highest Rayleigh numbers in which practically the half top of the cavity is hot and the half bottom is cold. This increase in Ra is like an increase in the volumetric thermal expansion coefficient, which means that density varies more with temperature. In other words, at very low Ra, the heat transfer is mainly by conduction, but as the Rayleigh number increases the differences in density become more important and the heat transport is by convection.

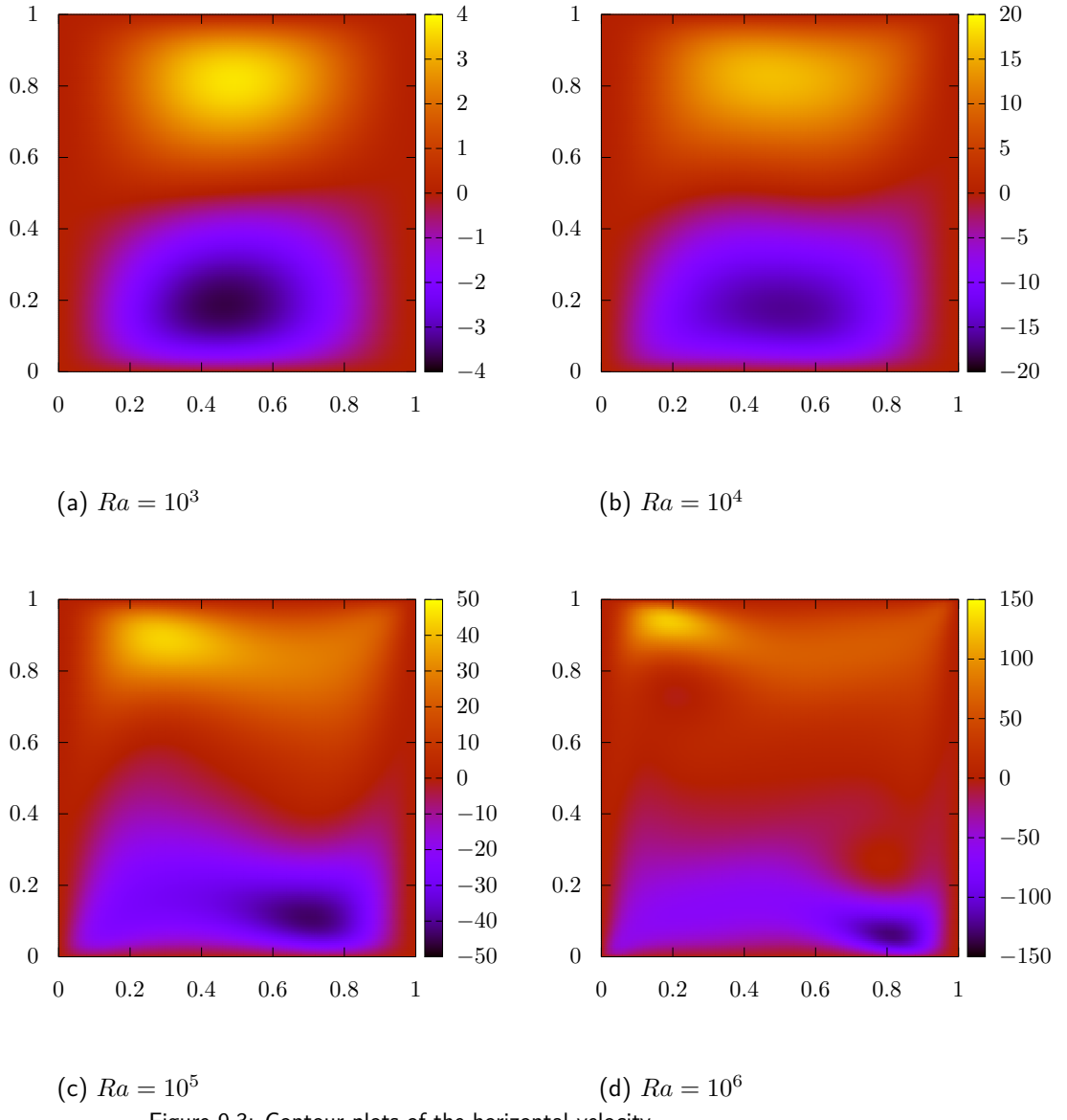


Figure 9.3: Contour plots of the horizontal velocity

Results

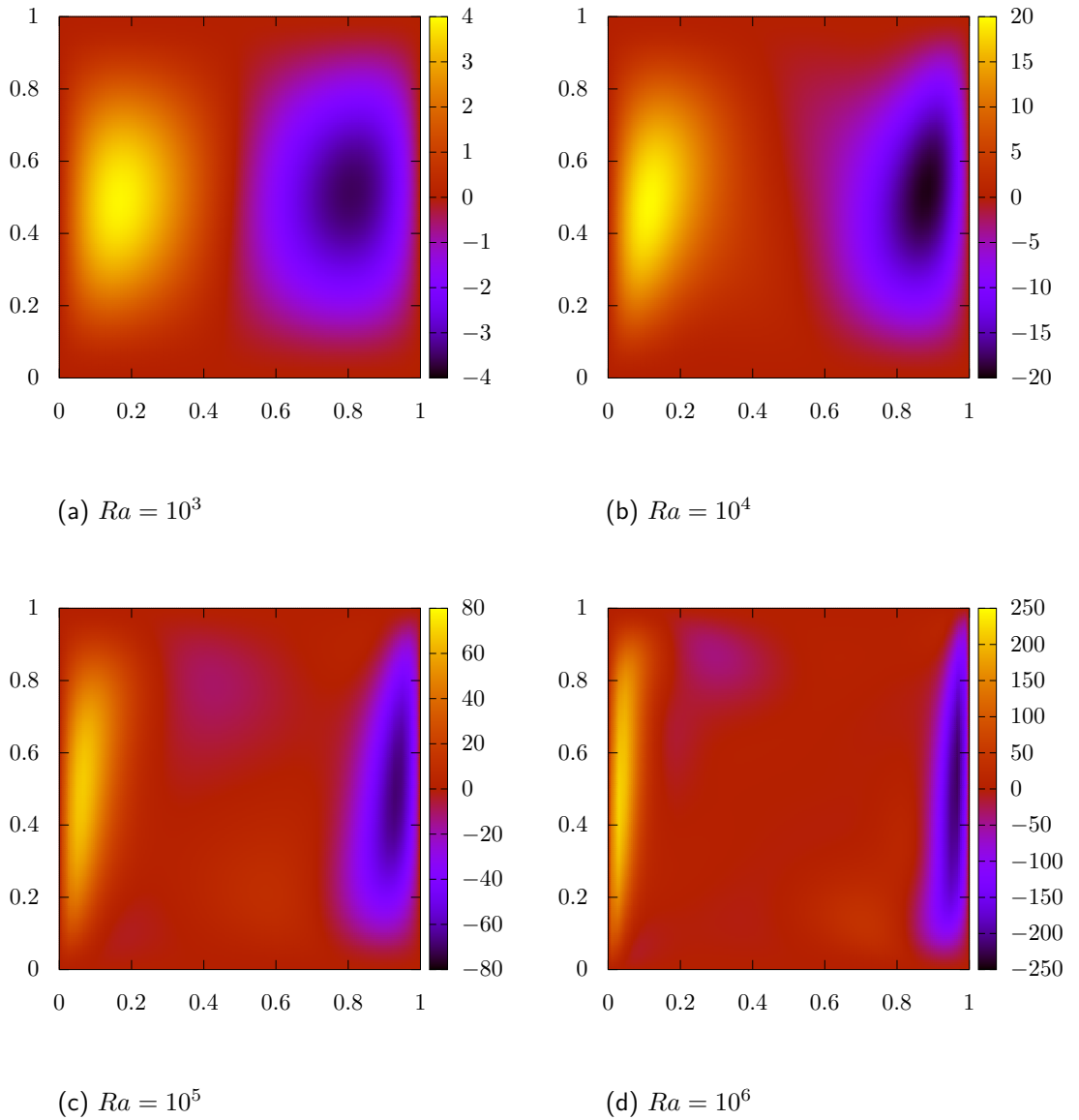


Figure 9.4: Contour plots of the vertical velocity

Figure 9.3 displays the horizontal velocity in the cavity for the studied Rayleigh numbers. In the case of the horizontal velocity, it can be seen that the hot fluid (in top) moves to the colder zone as expected, displacing the cold fluid (at the bottom) to the left. At low Rayleigh numbers, the maximum velocities, positive and negative, are in the top and bottom middle of the cavity; but at higher Ra, the maximum velocities move to the right and left corners respectively.

Regarding the vertical velocity (figures 9.4), the highest values are obtained near the walls. The hot fluid (left) moves upwards, whereas the cold fluid (right), that has a higher density, moves downwards. In the centre of the cavity there is also vertical movement, but at lower

Results

velocities. When the Rayleigh number increases, the areas with high vertical velocities are stretched, increasing the velocity gradient in the walls. It is also important to notice that in figures 9.4c and 9.4d there is some downwards movement in the left half of the cavity and a weak upwards movement in the bottom right, suggesting that the motion of the fluid becomes more complex at higher Ra.

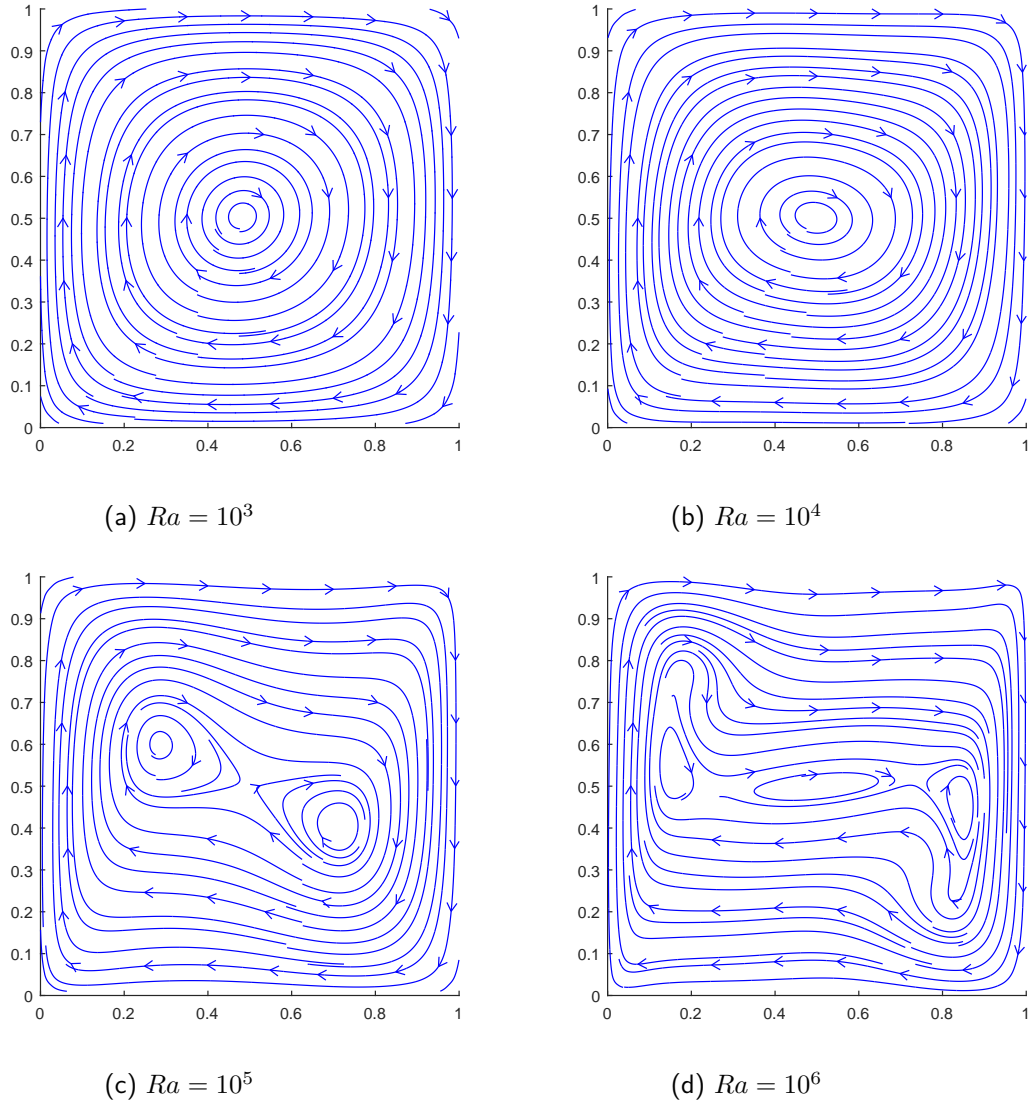


Figure 9.5: Streamlines of the flow in the heated cavity

As a conclusion, regarding the horizontal and vertical velocities, it can be said the the fluid moves in a clock-wise direction, as it can be seen in figure 9.5. At lower Ra, when the heat transfer is mainly by conduction, the fluid rotates around the centre of the cavity. However, as the Rayleigh number increases and convection becomes more important, the rotation is more complex. The central vortex stretches until it divides in two vortices, changing the motion of the fluid.

Results

Finally, a verification of the results has to be done. Table 9.3 displays a comparison between the results obtained with the code and the reference values [9]. The parameters studied are listed below:

- u_{max} : Maximum horizontal velocity on the vertical mid-plane of the cavity and its location.
- v_{max} : Maximum vertical velocity on the horizontal mid-plane of the cavity and its location.
- \overline{Nu} : Average Nusselt number throughout the cavity.
- $Nu_{1/2}$: Average Nusselt number on the vertical mid-plane of the cavity.
- Nu_0 : Average Nusselt number on the vertical boundary of the cavity at $x = 0$.
- Nu_{max} : Maximum value of the local Nusselt number on the left wall $x = 0$ and its location.
- Nu_{min} : Minimum value of the local Nusselt number on the left wall $x = 0$ and its location.

	$Ra = 10^3$		$Ra = 10^4$		$Ra = 10^5$		$Ra = 10^6$	
	Calculated	Bench	Calculated	Bench	Calculated	Bench	Calculated	Bench
u_{max}	3.708	3.649	16.198	16.178	34.508	34.73	66.192	64.63
y	0.81	0.813	0.83	0.823	0.85	0.855	0.85	0.85
v_{max}	3.908	3.697	19.648	19.617	68.663	68.59	220.23	219.36
x	0.17	0.178	0.11	0.119	0.07	0.066	0.03	0.038
\overline{Nu}	1.122	1.118	2.244	2.243	4.535	4.519	9.031	8.8
$Nu_{1/2}$	1.095	1.118	2.228	2.243	4.536	4.519	9.110	8.799
Nu_0	1.367	1.117	2.331	2.238	4.669	4.509	9.419	8.817
Nu_{max}	1.795	1.505	3.626	3.528	8.045	7.717	20.019	17.925
y	0.09	0.092	0.15	0.143	0.07	0.081	0.03	0.038
Nu_{min}	0.873	0.692	0.616	0.586	0.764	0.729	1.062	0.989
y	1	1	1	1	1	1	1	1

Table 9.3: Comparison between the benchmark solution and the calculated one [9]

In some cases the error can be bigger than 5%, especially in the Nusselt numbers on the left wall and in the locations of the values. In the case of the coordinates, the error may be due to the mesh used. In the calculations the mesh was coarser than the one used in the reference solution. All in all, the results that have higher error are the ones of the lowest and highest Rayleigh numbers.

10 | Burgers' equation

The Reynolds number of a flow measures the relative importance of inertia and viscous forces. If it is below the critical Reynolds number, the flow is smooth and regular, it is a laminar flow. If the Reynolds number is above the critical Reynolds, the flow becomes random and chaotic. It becomes a turbulent flow [11].

Unfortunately, turbulence is the usual state of motion of the fluids, except at very low Reynolds numbers. When the Reynolds number is high, the inertial forces lead to instabilities. In this regime, the properties of the flow are irregular, with three-dimensional fluctuations [12]. These turbulent motions are rotating swirls named eddies.

There are different scales of eddies in a turbulent flow [13]. The large ones control the transport and mixing in the flow, and are influenced by the geometry. On the other hand, small eddies depend on the energy that receive from the large scales and on the viscosity. Large eddies are unstable and tend to break, transferring their energy to smaller eddies. These smaller eddies also break, transferring their spectral energy to even smaller eddies, and so on. This process of energy transfer to smaller scales is called energy cascade.

As a consequence, depending on their size, eddies have different energy. Typically, energy is injected in the larger scales. This is called the production range. Then, in the inertial range, there is a transfer of energy from larger scales to smaller ones. In this range, the motion of the eddies is determined by the inertial effects, with viscosity still being negligible. And, finally, in even smaller scales, the energy is dissipated due to the viscous effects. This process is represented in figure 10.1.

In conclusion, turbulence is very complex. It requires to model different scales, and to take into account non-linear effects. Navier-Stokes equations can describe this non-linearity of turbulence, but their numerical simulation is difficult. Moreover, since the scale of the eddies can become really small, the number of control volumes required in the simulation would be very high, and the resulting code would be computationally expensive. To simplify the calculations, Burgers proposed a one-dimensional model for turbulence: the Burgers' equation.

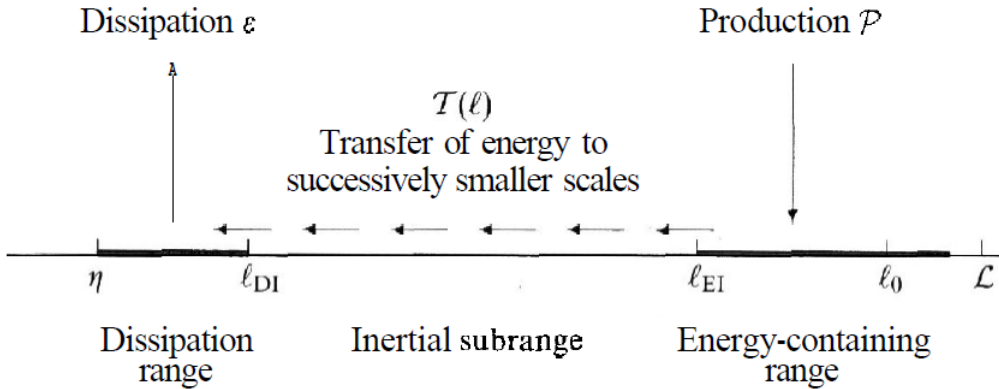


Figure 10.1: Schematic diagram of the energy cascade as a function of the size of the eddies. Extracted from [13]

10.1 Burgulence

Burgers' equation, also known as Burgulence, is a one dimensional approach to the momentum equation in an incompressible flow. It is the simplest equation that combines non-linearity and dissipation [14]. Its non-dimensional expression is:

$$\frac{\partial u}{\partial t} + u \frac{\partial u}{\partial x} = \frac{1}{Re} \frac{\partial^2 u}{\partial x^2} + f \quad (10.1)$$

where u is the velocity in the studied dimension, Re the Reynolds number and f the source term.

Since the equation is one-dimensional, the continuity equation is removed. The pressure gradient is also removed because it depends on the continuity equation.

10.2 Fourier space

The easiest way to solve the equation is to solve it in Fourier space. The basic approach of this space is that any function can be represented as a sum of sinus and cosines known as Fourier series in the following way:

$$u(x) = \sum_{k=-\infty}^{k=+\infty} \hat{u}_k e^{ikx} \quad (10.2)$$

where $e^{ikx} = \cos(kx) + i \sin(kx)$, with $k = 2\pi/l$ being the wavenumber, a parameter that depends on the length of the eddies.

Nonetheless, in a numerical calculation, it is impossible to have an infinite number of terms, it is necessary to have a finite number. Fortunately, in spectral methods the biggest amount of

information is in the lowest frequencies, which means that it is not necessary to have a huge amount of terms in order to have a proper solution of the equation. Taking this into account, the functions that are represented in the Fourier space become a sum of a finite number of sinus and cosines:

$$u(x) = \sum_{k=-N}^{k=+N} \hat{u}_k e^{ikx} \quad (10.3)$$

Using this expression, the Burgers' equation can be transformed into the Fourier space. However, the derivatives have to be calculated. Applying the derivative to the Fourier function definition:

$$\frac{\partial u}{\partial x} = \frac{\partial}{\partial x} \sum_{k=-N}^{k=+N} \hat{u}_k e^{ikx} = \sum_{k=-N}^{k=+N} \hat{u}_k \frac{\partial e^{ikx}}{\partial x} = \sum_{k=-N}^{k=+N} \hat{u}_k (ik) e^{ikx} \quad (10.4)$$

The same procedure is applied to the second derivative in order to obtain the diffusive term:

$$\begin{aligned} \frac{\partial^2 u}{\partial x^2} &= \frac{\partial}{\partial x} \left(\frac{\partial u}{\partial x} \right) = \frac{\partial}{\partial x} \sum_{k=-N}^{k=+N} \hat{u}_k (ik) e^{ikx} = \sum_{k=-N}^{k=+N} \hat{u}_k (ik) \frac{\partial e^{ikx}}{\partial x} = \\ &\quad \sum_{k=-N}^{k=+N} \hat{u}_k (ik)^2 e^{ikx} = \sum_{k=-N}^{k=+N} (-k^2 \hat{u}_k) e^{ikx} \end{aligned} \quad (10.5)$$

The transient 10.6 and forcing 10.7 terms are straightforward:

$$\frac{\partial u}{\partial t} = \frac{\partial}{\partial t} \sum_{k=-N}^{k=+N} \hat{u}_k e^{ikx} \quad (10.6)$$

$$f = \sum_{k=-N}^{k=+N} F_k e^{ikx} \quad (10.7)$$

On the other hand, the convective term is more complicated. This non-linear term is a multiplication of the function u and its derivative, and when it is transformed into Fourier space there are some things that need to be taken into account. The terms in question are:

$$\frac{\partial u}{\partial x} = \sum_{q=-N}^{q=+N} iq \hat{u}_q e^{iqx} \quad (10.8)$$

$$u = \sum_{p=-N}^{p=+N} \hat{u}_p e^{ipx} \quad (10.9)$$

As it is noted, the variable k has been renamed in both terms in order to avoid confusions when the expressions are multiplied to obtain the convective term. It is finally calculated as:

$$u \frac{\partial u}{\partial x} = \sum_{p,q} \hat{u}_p iq \hat{u}_q e^{i(p+q)x} \quad (10.10)$$

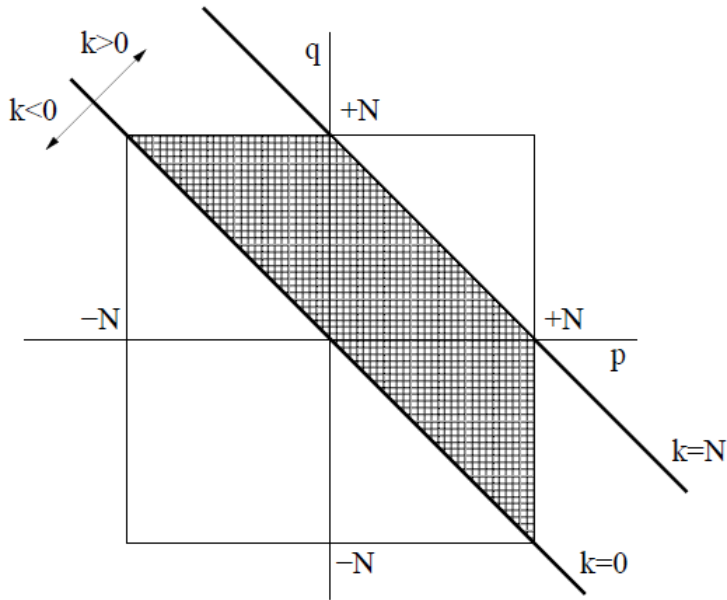


Figure 10.2: Representation of all the possible interactions between the modes in the convective term. Extracted from [15]

Taking all these expressions, integrating them into the Burgers equation and applying the Fourier transform, the final expression is:

$$\frac{\partial \hat{u}_k}{\partial t} + \sum_{p+q=k} \hat{u}_p i q \hat{u}_q = -\frac{k^2}{Re} \hat{u}_k + F_k \quad (10.11)$$

for $k = 1, \dots, N$; and where $\hat{u}_k \in \mathbb{C}$.

One of the main advantages of spectral methods is that all the modes can be solved separately. However, due to the convective term, there is still a sum of terms in the equation, named triadic interactions. This summation can be easily interpreted with figure 10.2. In Fourier space $\hat{u}_{-k} = \hat{u}_k$, so only the positive modes need to be solved. Moreover, since the Fourier series are truncated for $k \leq |N|$, the only possible interactions are those of $p + q \leq N$. Therefore, only the interactions between the lines $k = 0$ and $k = +N$ have to be considered in the computation of the convective term.

10.3 Discretization

In order to solve the equation it is necessary to discretize it over time. The time-integration scheme used is the fully explicit one:

$$\frac{\hat{u}_k^{n+1} - \hat{u}_k^n}{\Delta t} + \sum_{p+q=k} \hat{u}_p i q \hat{u}_q = -\frac{k^2}{Re} \hat{u}_k + F_k \quad (10.12)$$

However, the time step needs to be small enough to guarantee good results. A CFL-like condition is imposed:

$$\Delta t \leq C_1 \frac{Re}{N^2} \quad (10.13)$$

The calculation of the kinetic energy as a function of the wavenumber is simply done as:

$$E_k = |\hat{u}_k|^2 \quad (10.14)$$

10.3.1 Direct Numerical Simulation

The direct application of the equation 10.12 to obtain \hat{u}_k^{n+1} is called Direct Numerical Simulation (DNS). It is the simplest method, and it does not use any model approximation. However, in order to provide accurate results, several modes of the equation have to be solved.

10.3.2 Large-Eddy Simulation

A method that can improve the calculations of the DNS is the Large-Eddy Simulation (LES). Like DNS, it starts with a one-dimensional equation in which the unknown is not the velocity but its average.

$$\frac{\partial \bar{u}}{\partial t} + \bar{u} \frac{\partial \bar{u}}{\partial x} = \frac{1}{Re} \frac{\partial^2 \bar{u}}{\partial x^2} + f - \frac{\partial}{\partial x} \tau(u) \quad (10.15)$$

where

$$\tau(u) = \bar{u}^2 - \bar{u}^2 \quad (10.16)$$

In the model proposed by Smagorinsky, this subfilter tensor is modeled using a viscosity called the eddy-viscosity [15]:

$$\tau(u) \approx \nu_t \frac{\partial \bar{u}}{\partial x} \quad (10.17)$$

The Smagorinsky model also proposes an expression for ν_t , but it cannot be applied in Fourier space. To do so, a spectral viscosity model is used:

$$\nu_t(k/k_N) = \nu_t^{+\infty} \left(\frac{E_{k_N}}{k_N} \right)^{1/2} \nu_t^* \left(\frac{k}{k_N} \right) \quad (10.18)$$

with

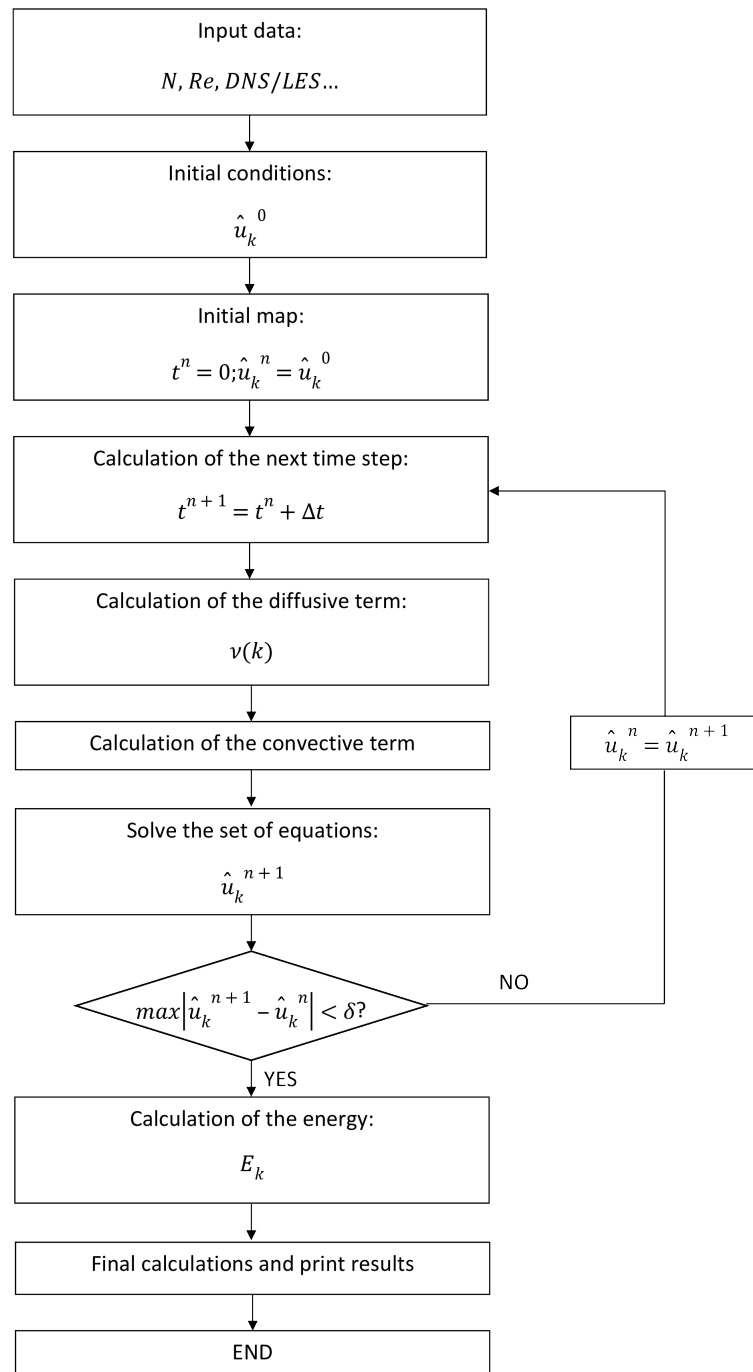
$$\nu_t^{+\infty} = 0.31 \frac{5-m}{m+1} \sqrt{3-m} C_K^{-3/2} \quad (10.19)$$

$$\nu_t^* \left(\frac{k}{k_N} \right) = 1 + 34.5 e^{-3.03(k_N/k)} \quad (10.20)$$

where m is the slope of the energy spectrum, E_{k_N} is the energy at the truncated frequency k_N , and C_K is the Kolmogorov constant. With the results obtained with the DNS, it can be deduced that $m \approx 2$. And for the value of the Kolomogorov constant, it is known that for the one-dimensional Burgers' equation it is $C_K \approx 0.4523$.

10.4 Algorithm

A scheme of the algorithm used to solve the Burgers' equation is displayed below. The problem ends when the simulation reaches a steady state.



10.5 Results

In order to obtain the energy cascade, the Burgers' equation has been solved using DNS and LES. The following results are studied for $Re = 40$, taking as initial conditions:

$$\hat{u}_k = k^{-1} \quad (10.21)$$

Figure 10.3 represents the energy cascade in a logarithmic plot. As the wavenumber k increases (the length of the eddies decreases), the kinetic energy decreases. For bigger eddies, inertia makes the flow more chaotic and the energy is higher, but as their length decreases, the viscosity becomes more important and the energy is reduced.

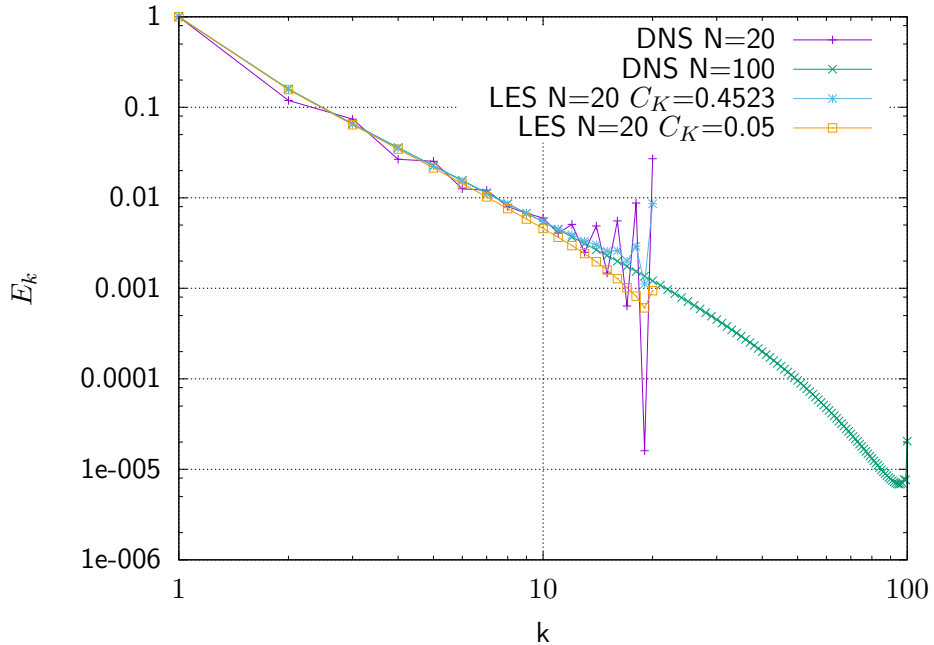


Figure 10.3: Energy spectrum of the steady-state solution of the Burgers' equation

As it can be seen, different simulations have been computed. In the case of the DNS, the results are obtained using 20 modes and 100 nodes. For $N = 20$, the solution is not really precise, some more nodes have to be computed. However, the results for $N = 100$ are more accurate.

In the case of LES, even with less nodes, the results are better. For $C_K = 0.4523$, the solution is very similar to that obtained in the case of $N = 100$ using DNS for low wavenumbers. With the same number of nodes, the results are better, even though the calculations are more complicated.

11 | Square cylinder

The square cylinder problem studies the two-dimensional laminar flow around a square cylinder inside a plane channel. The description of the problem can be seen in figure 11.1.

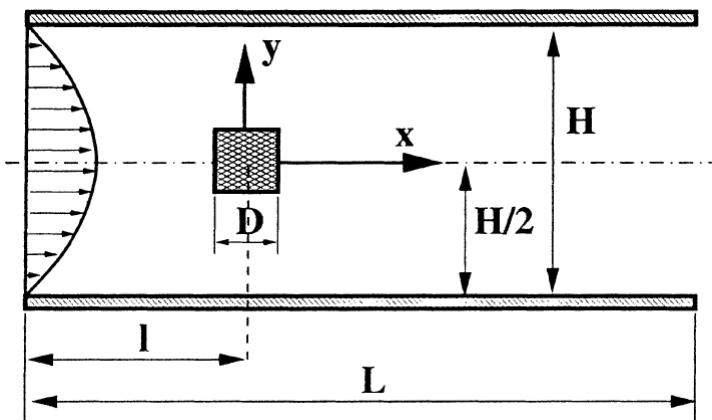


Figure 11.1: General scheme of the square cylinder problem. Extracted from [16]

11.1 Discretization

In this kind of problem, the region near the cylinder has an important pressure and velocity gradient whereas in the rest of the channel flow they are smoother. So, near the cylinder a finer mesh is needed, but not in the whole domain of the problem. Using a very fine mesh in all the channel would be computationally expensive and inefficient, but a coarser mesh would lead to inaccurate results, especially in the cylinder.

The domain is divided in three parts, vertically and horizontally. The mesh that contains the obstacle is a uniform mesh of very high precision, whereas the other meshes are also uniform but coarser. The details of the discretization are in table 11.1.

N_1	N_2	N_3	M_1	M_2	M_3	D	H	L	l	ρ	u_{max}	δ
90	10	300	30	10	30	1	$8D$	$50D$	$L/4$	1	1	10^{-4}

Table 11.1: Numerical parameters of the square cylinder problem

11.2 Boundary conditions

11.2.1 Inlet conditions

Since the flow is inside a channel, the inflow has a parabolic velocity profile with a maximum velocity u_{max} in the centre:

$$u(y) = 4u_{max} \left[\left(\frac{y}{H} \right) - \left(\frac{y}{H} \right)^2 \right] \quad (11.1)$$

This maximum velocity defines the Reynolds number of the problem:

$$Re = Re_{max} = \frac{\rho u_{max} D}{\mu} \quad (11.2)$$

As for the pressure conditions, a Neumann condition is imposed:

$$\frac{\partial p}{\partial x} = 0 \quad (11.3)$$

11.2.2 Outlet conditions

In order to have a developed flow in the outlet, it is important to have a distance large enough between the position of the cylinder and the end of the channel in order to have fully developed flow. To define the outflow, a convective boundary condition is used:

$$\frac{\partial u}{\partial t} + u_{conv} \frac{\partial u}{\partial x} = 0 \quad (11.4)$$

where u_{conv} is equal to the maximum velocity u_{max} of the parabolic inflow velocity profile. The integration over time of this condition is done using an Adams-Bashforth scheme.

In the outlet, as opposite to the inlet, a Dirichlet condition is used to determine the pressure:

$$p = 0 \quad (11.5)$$

11.2.3 Wall conditions

In the channel walls the no-slip condition is applied:

$$\vec{v} = 0 \quad (11.6)$$

As well as the boundary layer condition, in which the pressure gradient normal to the wall is 0.

In the convection problems studied in the previous sections the flow was developing inside a cavity with no other obstacles than the walls. In this problem, the fluid flows around a square cylinder, so the boundary conditions have to be also implemented for the cylinder. Since it is a solid object and it does not allow air to flow through it, it is treated as a wall [1]. Consequently the velocity in its boundary is also given by equation 11.6.

11.3 Algorithm

The algorithm used in the resolution of this problem is the same used in the calculation of the driven cavity problem (section 8.3).

11.4 Results

Depending on the Reynolds number the wake of the cylinder is completely different. In the following results, the fluid is only studied for $1 \leq Re < 60$, the steady regime. For $Re \geq 60$ the fluid changes completely its behaviour and never reaches a steady state. It is called the unsteady regime.

Figure 11.2 shows the distribution of the horizontal velocity as a function of the Reynolds number. When the fluid reaches the cylinder it slows down, but when it is passing it the flow accelerates. In the rear side of the cylinder there is a zone with negative velocity. As the Re increases the accelerated area and the zone with reverse flow increase as well. Regarding the general distribution of velocities, for low Re it is almost symmetric, but as the Re increases it stretches to the right.

Regarding the vertical velocity (figure 11.3), in order to avoid the cylinder, the flow moves up near its upper edge and down near the lower edge. In the rear side of the cylinder the movement is completely the opposite. Again, for low Re the distribution is more or less symmetric, but as the Re increases it stretches to the right and the gradient of velocities in the frontal edges of the cylinder increases as well.

Finally, the fluid flow is completely defined by the streamlines of figure 11.4. At $Re = 1$ the flow passes the cylinder without separation. But passed $Re \approx 5$, two symmetric vortices appear in the rear side of the cylinder. The length of these vortices increases with the Reynolds number.

In conclusion, for low Re , viscosity avoids the separation of the laminar boundary layers. But as

Results

the Re increases and convection becomes more important there is a separation of the boundary layer in the rear side of the cylinder that generates the obtained symmetrical vortices.

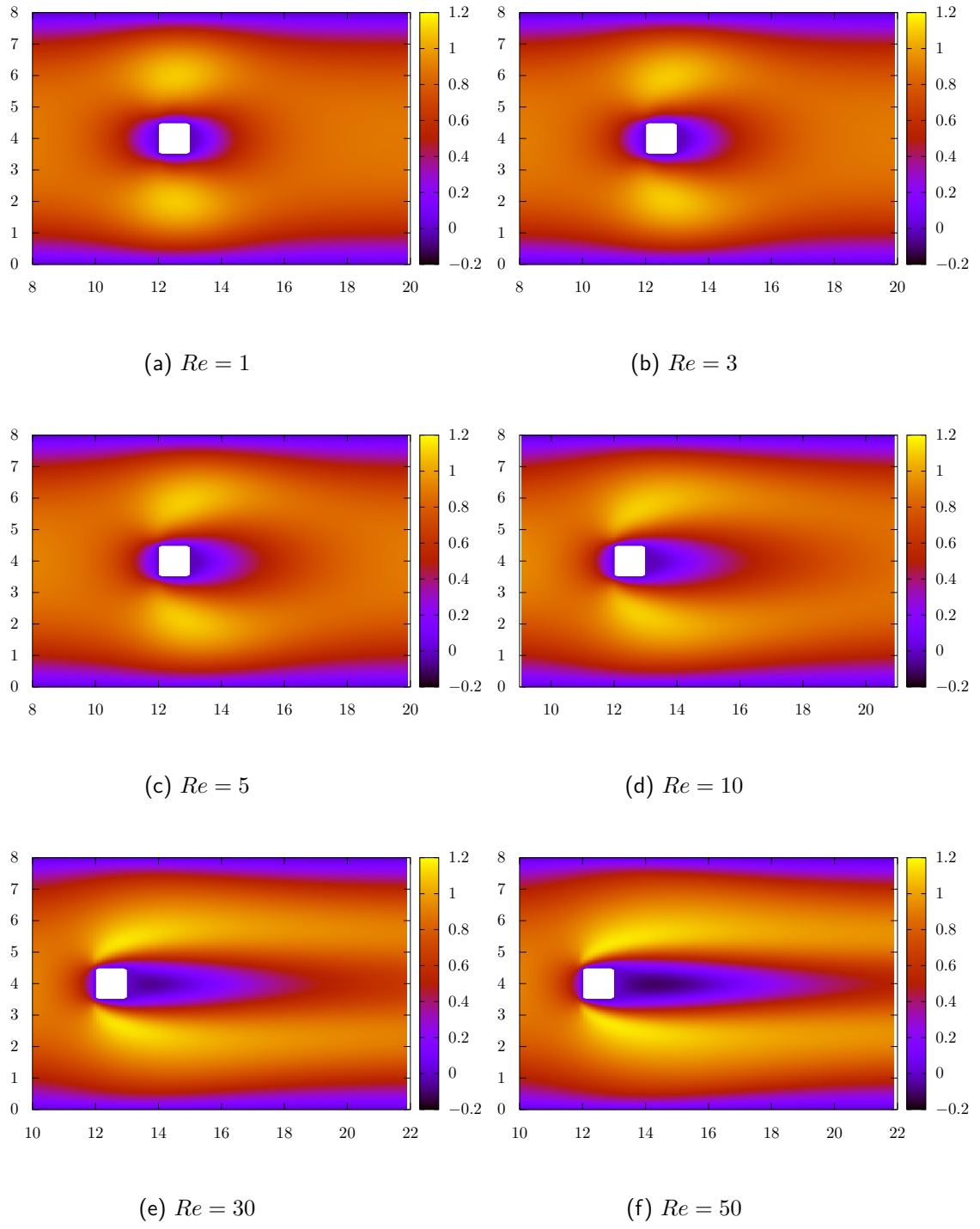


Figure 11.2: Horizontal velocity near the cylinder

Results

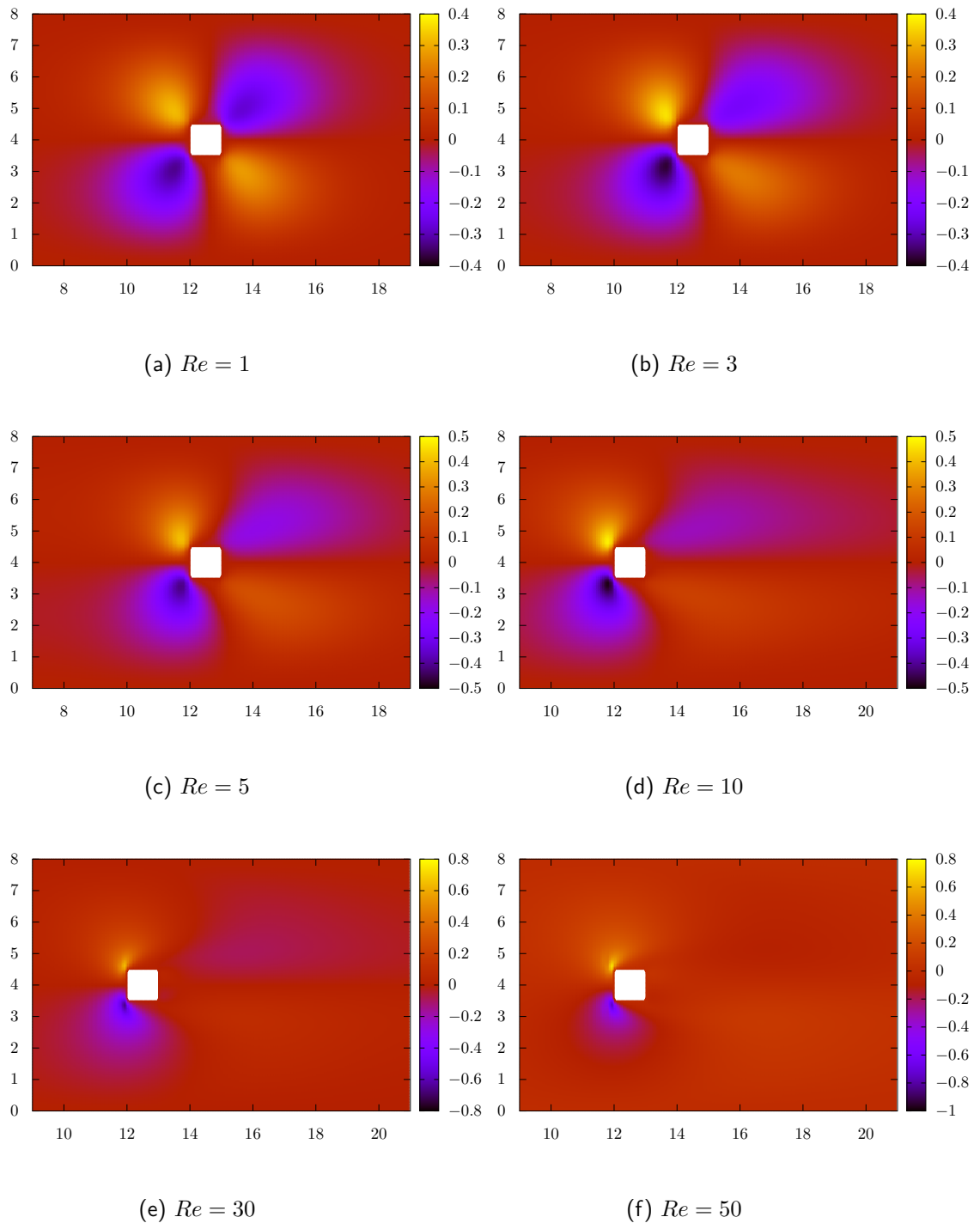
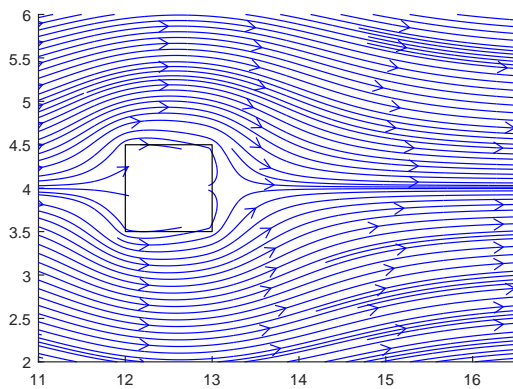
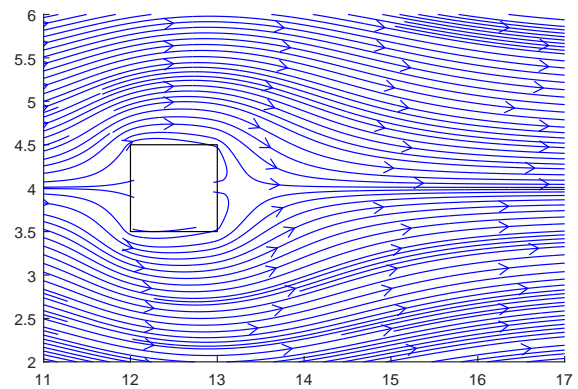


Figure 11.3: Vertical velocity near the cylinder

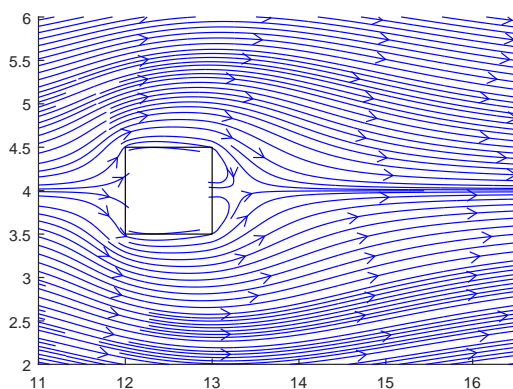
Results



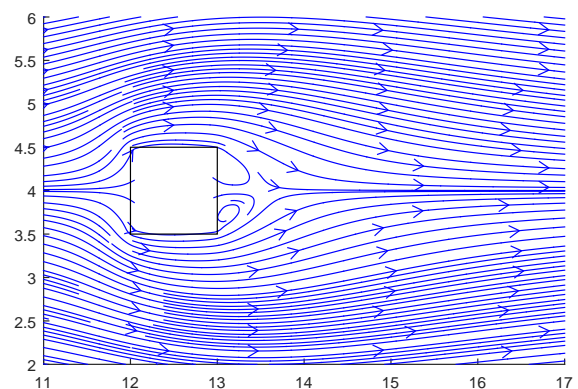
(a) $Re = 1$



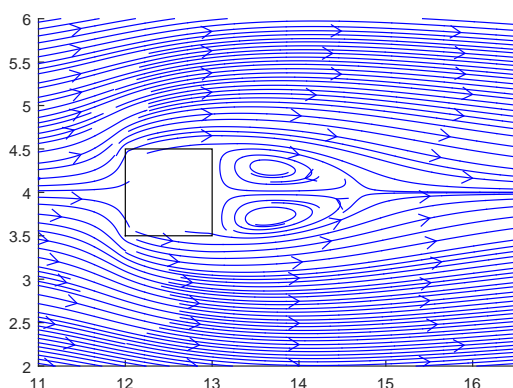
(b) $Re = 3$



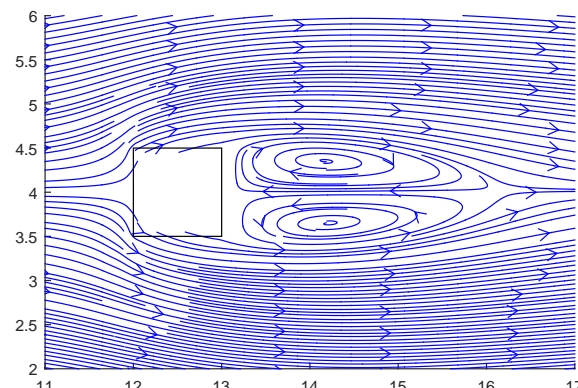
(c) $Re = 5$



(d) $Re = 10$



(e) $Re = 30$



(f) $Re = 50$

Figure 11.4: Vertical velocity near the cylinder

Results

An important parameter of the problems that study the flow around an object is the length of the closed wake behind the cylinder. According to [16], the recirculation length has a linear dependence on the Reynolds number:

$$L_r/D = -0.065 + 0.0554Re \quad \text{for } 5 < Re < 60 \quad (11.7)$$

The recirculation length is obtained comparing the horizontal velocities of the central horizontal plane. In the wake the velocity is negative, but in the external flow the velocity is positive. The recirculation length is the distance between the rear side of the cylinder and the point in which the velocity changes from negative to positive.

Figure 11.5 compares the calculated results with the reference ones as a function of the Reynolds number. The results are very similar, but at low Re the error is quite high. It could be due to the mesh. At low Re the recirculation length is very small, so it can only be accurately measured with a very fine mesh.

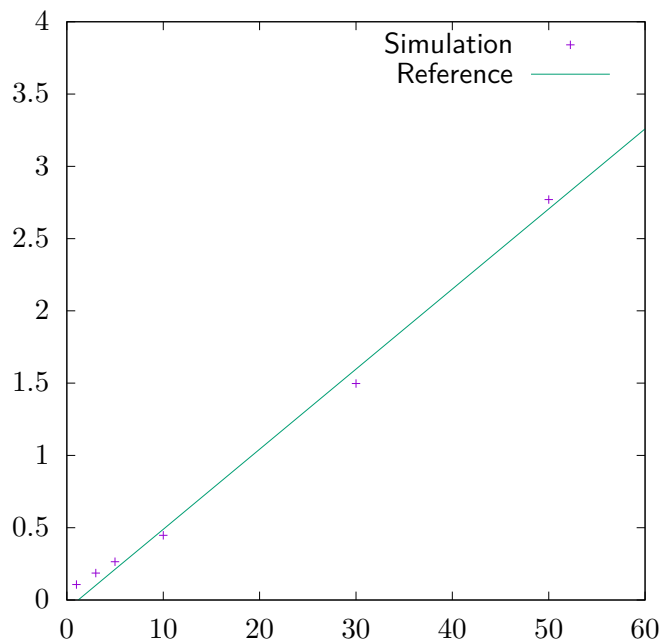


Figure 11.5: Recirculation length vs. Reynolds number

12 | Conclusions

This study was first proposed in order to improve the knowledge in the computational resolution of the conservation equations. To do so, a previous research on the state of the art of this field has been done. Then, some numerical methods have been studied, and in order to completely understand them they have been applied to different cases. All this, taking into account all the requirements.

The study of computational methods began with the concept of discretization and its application to differential equations. The simplest case, conduction, has served as an introduction to numerical solutions and unsteady problems. Secondly, the Smith-Hutton problem, has introduced the use of interpolation schemes. In the driven cavity problem, the fractional step method has been proposed. Then, the differentially heated cavity problem, that required the resolution of the momentum and energy equations, has served as an introduction to problems that combine the resolution of both equations. Finally, as a brief introduction to turbulence, spectral methods have been introduced to solve the Burgers' equation.

Concerning the results obtained with the simulations, they are realistic and similar to the reference values. There are some differences between the calculated values and the reference ones, but the error is not high. These discrepancies may appear due to the numerical methods used to solve the problem or the mesh refinement, among other causes.

Finally, all the knowledge acquired in this first part of the study has led to the resolution of a practical case: the flow around a square cylinder inside a channel. This case is more similar to an aerodynamics problem, which is one of the main disciplines of aerospace engineering, because it studies the behaviour of the external flow around an object.

In general, the simulation of the application case gave correct results, but it has only been implemented for low Reynolds number flows with steady solutions. The results obtained were accurate enough, with some discrepancies for very low Re flows.

Other remarkable achievement of this study is the acknowledgement of the importance of mesh refinement and code structuring. An appropriate mesh can be the difference between a simulation that does or does not work. On the other hand, a structured code is easier to

understand and facilitates the detection of errors.

12.1 Future work

To continue this study, the next step would be the adaptation of the actual code that calculates the external flow around a square cylinder to the resolution of higher Reynolds numbers. This would allow obtaining unsteady solutions, which would lead to the study of the von Kármán vortex streets.

Another major improvement that could be done to this program is the calculation of the aerodynamic coefficients of drag and lift in order to understand their dependence on the Reynolds number.

Other general improvements are the study of the most appropriate mesh for each case and the improvement of the codes to increase the overall efficiency of the simulations.

Finally, the next step in this study would be the development of a code to study the turbulence phenomenon.

13 | Economical, environmental and temporal considerations

13.1 Budget

The economical cost of this study is divided in three sections:

- Human resources: The study was developed by an aerospace engineering student during 300 hours. The human resources are the hours invested in the making of the study.
- Software: It refers to the programs used to develop the study: *TeXstudio 2.12.4*, *Dev-C++ 5.11*, *gnuplot 5.0*, *Matlab R2015a*, *Microsoft Excel 2010* and *Mendeley Desktop 1.17.9*.
- Hardware: One of the requirements of the study was that the developed codes had to be able to be executed in a normal computer. The hardware refers to the laptop used in the development of this study.

The total costs are summarized in table 13.1. To see more details refer to the Budget document.

Concept	Price	Units	Total
Human resources	15 €/hour	300 h	4,500 €
Software	148 €	1	148 €
Hardware	26 €/month	4 months	104 €
			4,752 €

Table 13.1: Total cost of the study

13.2 Environmental impact

In the making of this paper different cases were studied: conduction through a wall, the movement of a fluid inside a cavity, natural convection... With the use of computational methods these studies only required a computer to be conducted. As a consequence, it avoided an experimental release of the problems and the use of an appropriate installation to perform them. This aspect reduces considerably the environmental impact that the study could have had.

As for the resources used, the main tool was a computer and the electricity needed for its operation. However, in the making of this paper, these resources do not generate an additional environmental impact, because they are commonly used in a student's everyday life.

In short, the environmental impact of this study was minimum.

13.3 Planning

The planning of the tasks has had some modifications with respect to the proposal of the project charter. The main difference is that instead of including the study of radiation, the paper has focused on the resolution of convection, which was more related to the final case of study. For more information refer to Attachment C.

Regarding the future work proposed in section 12.1 the time estimation of the tasks is the following:

- Unsteady solutions of the square cylinder problem: 2 to 3 weeks
- Calculation of the aerodynamic coefficients: 1 week
- Mesh refinement and improvement of the codes: 4 weeks
- Development of a code to study the turbulence phenomenon: 7 to 8 weeks

14 | Bibliography

- [1] J. H. Ferziger and M. Peric. *Computational Methods for Fluid Dynamics*. Springer, Berlin, 3rd edition, 2002.
- [2] S. V. Patankar. *Numerical Heat Transfer and Fluid Flow*. McGraw-Hill, New York, 1980.
- [3] T. L. Bergman, A. S. Lavine, F. P. Incropera, and D. P. DeWitt. *Fundamentals of Heat and Mass Transfer*. John Wiley & Sons, 7th edition, 2011.
- [4] A. Bejan. *Convection Heat Transfer*. John Wiley & Sons, Hoboken, 4th edition, 2013.
- [5] CTTC. Introduction to the Fractional Step Method.
- [6] CTTC. Course on Numerical Methods in Heat Transfer and Fluid Dynamics Unit 4: Fractional Step Method Part1: Staggered Meshes.
- [7] U. Ghia, K. N. Ghia, and C. T. Shin. High-Re solutions for incompressible flow using the Navier-Stokes equations and a multigrid method. *Journal of Computational Physics*, 48:387–411, 1982.
- [8] G. de Vahl Davis and I. P. Jones. Natural convection in a square cavity: A comparison exercise. *International Journal for Numerical Methods in Fluids*, 3(July 1982):227–248, 1983.
- [9] G. de Vahl Davis. Natural convection of air in square cavity : A benchmark numerical solution. *International Journal for Numerical methods in Fluids*, 3(July 1982):249–264, 1983.
- [10] S. M. Ghiaasiaan. *Convective Heat and Mass Transfer*. Cambridge University Press, New York, 2011.
- [11] H. K. Versteeg and W. Malalasekera. *An Introduction to Computational Fluid Dynamics: The Finite Volume Method*. Pearson Education Limited, Harlow, 2nd edition, 2007.
- [12] CTTC. Turbulence Modelling from RANS to DNS and LES.
- [13] S. B. Pope. *Turbulent Flows*, volume 1. Cambridge University Press, 2000.

- [14] R. W. Johnson. *Handbook of Fluid Dynamics*. CRC Press, 2nd edition, 2016.
- [15] CTTC. Burgers' equation in Fourier space, 2014.
- [16] M. Breuer, J. Bernsdorf, T. Zeiser, and F. Durst. Accurate computations of the laminar flow past a square cylinder based on two different methods: Lattice-Boltzmann and finite-volume. *International Journal of Heat and Fluid Flow*, 21(2):186–196, 2000.